Multiproxy analysis of paleoenvironmental, paleoclimatic and paleoceanographic changes during the early Danian in the Caravaca section (Spain)

Vicente Gilabert[a,*], Ignacio Arenillas[a], José A. Arz[a], Sietske J. Batenburg[b], Stuart A. Robinson[c]

[a] Departamento de Ciencias de la Tierra, and Instituto Universitario de Investigación en Ciencias Ambientales de Aragón, Universidad de Zaragoza, E-50009 Zaragoza, Spain. C/ Pedro Cerbuna 12, 50009 Zaragoza. vgilabert@unizar.es, ias@unizar.es, josearz@unizar.es

[b] Departament de Dinàmica de la Terra i de l'Oceà, Facultat de Ciències de la Terra, Universitat de Barcelona, Martí i Franqués, 08028 Barcelona, Spain. sbatenburg@ub.edu

[c] Department of Earth Sciences, University of Oxford, South Parks Road, Oxford, OX1 3AN, UK. stuart.robinson@earth.ox.ac.uk

* Corresponding author Email address: vgilabert@unizar.es

ABSTRACT

After the Chicxulub impact and mass extinction at the Cretaceous-Paleogene boundary (K-PgB), ecosystems haltingly recovered under unstable conditions. An early Danian (65.9 Ma) perturbation of the carbon cycle known as Dan-C2, which includes two carbon isotopic excursions (CIEs), has been ascribed to inputs of greenhouse gases through large-scale volcanism of the Deccan Traps. However, the relationship between Dan-C2, volcanism and environmental and climatic changes during the early Danian remains ambiguous. Based on stable isotopes, calcium carbonate content, magnetic susceptibility and planktic foraminifera, we present a paleoenvironmental, paleoclimatic and paleoceanographic reconstruction of the early Danian from the Caravaca section, Spain, one of the most complete and continuous K-PgB sections

worldwide. The paleobiological response of planktic foraminifera suggests very volatile environmental conditions during the first 230 kyr of the Danian, as reflected in the rapid succession of opportunistic/generalist blooms and episodic high occurrences of aberrant specimens. According to our age model, the Dan-C2 has been identified at the Caravaca section from 65.92 to 65.74 Ma. No evidence of strong carbonate dissolution through ocean acidification was observed in the Dan-C2 interval or the rest of the studied section, excluding the K-PgB clay bed. We find that blooms of highly eutrophic *Chiloguembelitria* and increases in aberrant planktic foraminifera coincided with a major early Danian eruptive episode of Deccan Traps (Ambelani Formation), occurring before the Dan-C2. Conversely, during both Dan-C2 CIEs, less opportunistic taxa thrived, indicating changes in the upper part of the water column. This study demonstrates that the relationship between marine biota and climate change was very complex and rapidly changing during the early Danian. In addition, we propose that the Deccan volcanism had adverse effects on marine plankton, mostly through strong eutrophication, while an increased water column stratification during the Dan-C2 event resulted in a transient boost in the recovery of ecosystems.

HIGHLIGHTS

- Rapid changes among planktic foraminifera within the first 230 kyr of the Paleocene
- Low carbonate dissolution in the Danian suggests low rates of volcanic CO_2 emissions
- Evidence of the Dan-C2 event between 65.92 and 65.74 Ma
- Dan-C2 CIEs associated with reorganization of planktic foraminiferal assemblages

KEYWORDS

Deccan volcanism; Dan-C2; acme-stage; mass extinction; western Tethys

1. Introduction

The Cretaceous-Paleogene boundary (K-PgB) is marked by one of the most devastating geological events that has occurred on Earth (Alvarez et al., 1980; Smit and Hertogen, 1980) caused by the impact of a ~10 km-diameter asteroid at the Yucatan Peninsula, Mexico, known as the Chicxulub asteroid (Hildebrand et al., 1991). It is widely understood that the asteroid impact caused a series of catastrophic environmental effects, including the blockage of solar radiation leading to a cold and dark "impact winter", ocean acidification, and pollution by toxic heavy metals, resulting in one of the greatest biotic crises on Earth (Kring, 2007; Premović, 2009; Schulte et al., 2010; Vellekoop et al., 2014, 2016; Gulick et al., 2019; Henehan et al., 2019; Gibbs et al., 2020). The environmental effects were lethal in the pelagic realm and caused the decimation of calcareous plankton at the K-PgB (Smit, 1982; Arenillas et al., 2000a,b; Bown, 2005). Multiple lines of evidence have pointed to the Chicxulub impact as the main cause of the K-PgB mass extinction (e.g. Smit, 1999; Arenillas et al., 2006; Schulte et al., 2010; Lowery et al., 2018; Henehan et al., 2019). Nonetheless, recent advances in radiometric dating constrain the eruptive phases of Deccan Traps volcanism (in India), as well as the Chicxulub impact, to a period of only a few hundred thousand years during magnetochron C29r (Chenet et al., 2007; Renne et al., 2015; Schoene et al. 2015, 2019; Sprain et al., 2019) thereby hindering a clear distinction between the specific roles of volcanism and impact in the K-PgB mass extinction. Consequently, these issues remain a topic of intense debate 40 years since the impact hypothesis was first proposed (Alvarez et al., 1980; Hull et al., 2020; Keller et al., 2020).

Discrepancies in the age of the K-PgB and its stratigraphic position within the Deccan Traps, as well as uncertainty regarding the eruptive rates of its main phases, result in two models of Deccan Traps eruptions, and a controversy about the role of Deccan volcanism in the K-PgB mass extinction and early Danian climate change (Burgess, 2019; Hull et al., 2020; Keller et al., 2020). Based on $^{40}Ar/^{39}Ar$ dating, and volcano-stratigraphic and biostratigraphic evidence, it has been argued that the most voluminous Deccan eruptions occurred during the early Danian,

corresponding to the emplacement of the Poladpur, Ambenali and Mahabaleswar Formations of the Wai subgroup (Jay and Widdowson, 2008; Renne et al., 2015; Richards et al., 2015; Sprain et al., 2019). However, based on U/Pb dating of the Deccan Traps Formations, it has been proposed that the volcanic phase with the highest eruptive rate (Poladpur Formation) occurred in the latest Maastrichtian, only tens of thousands of years prior the K-PgB (Schoene et al., 2015, 2019, 2021).

Although geochemical signatures ascribed to Deccan volcanism, such as $^{187}Os/^{188}Os$ excursions and Hg enrichments, have been recognized prior to the KPB (Robinson et al., 2009; Font et al., 2016,2018; Keller et al., 2020), several paleo-ecological and paleoclimate studies (e.g. Thibault and Gardin, 2010; Thibault et al., 2016; Hull et al., 2020; Gilabert et al., 2021) have shown that the influence of the Deccan volcanism during the latest Maastrichtian did not contribute to the K-PgB mass extinction (although this is disputed by some; e.g. Keller et al., 2020 and references therein). A broad temporal coincidence also exists between post-K-PgB Deccan volcanism and the first Danian hyperthermal event, known as Dan-C2 (Quillévéré et al., 2008), which has led some to speculate that the two are mechanistically linked (e.g. Coccioni et al., 2010; Punekar et al., 2014a; Krahl et al., 2020). However, others have suggested that the Dan-C2 event could be astronomically controlled (Quillévéré et al., 2008; Barnet et al., 2019; Sinnesael et al., 2019) and recent models of the CO_2 emission rates of Deccan volcanism suggest that outgassing from Deccan volcanism alone was incapable of driving the magnitude of climate change observed during the early Danian (Hull et al., 2020; Fendley et al., 2020).

During the earliest Danian, planktic foraminiferal and calcareous nannoplankton assemblages were characterized by low diversity, a high single-species dominance, rapid evolutionary turnovers, and blooms of smaller generalist or opportunist taxa that could thrive under eutrophic and unstable conditions (Romein, 1977; Smit, 1982; Huber et al., 2002; Lamolda et al., 2005; Arenillas et al., 2006; Jiang et al., 2010; Jones et al., 2019; Lowery et al., 2020). Recently, it has been proposed that non-calcareous algal and microbial communities bloomed in the open ocean in the short-term aftermath of the Chicxulub impact (Bralower et al., 2020).

According to Bralower et al. (2020), these microbial blooms probably contributed to rapid ecosystem recovery by removing nutrients and providing a food source for higher trophic orders, enhancing pelagic ocean habitability as evidenced by the rapid recovery of planktic foraminifera and calcareous nannoplankton after the impact.

The main planktic foraminiferal indicators of enhanced environmental stress across the K-PgB are the guembelitriid blooms (Kroon and Nederbragt 1990; Keller and Pardo, 2004; Pardo and Keller, 2008; Ashckenazi-Polivoda et al., 2014; Punekar et al., 2014a,b) and the increases in aberrant planktic foraminifera tests (Gerstel et al., 1986; Coccioni and Luciani, 2006; Arenillas et al., 2018). Worldwide, blooms of *Guembelitria* and its descendant *Chiloguembelitria* have been reported well above the K-PgB (Arenillas et al., 2018), and thus appear genetically disconnected from the Chicxulub impact. However, the blooms did occur within the temporal range of Deccan volcanism in the Danian which points to a potential cause and effect relationship (Keller et al., 2012; Punekar et al., 2014a,b; Arenillas et al., 2018). Similarly, an increase in aberrant foraminifera tests after the K-PgB has been shown to continue locally at the El Kef and Aïn Settara sections (Tunisia) for several hundreds of thousands of years after the K-PgB (Arenillas et al., 2018), suggesting the persistence of stressed conditions.

Except for the immediate aftermath of the Chicxulub impact, the climatic and environmental changes that occurred during the first thousand years of the Danian leading up to the Dan-C2 event have not been exhaustively examined (e.g., Quillévéré et al., 2008; Barnet et al., 2019). To improve our understanding of the complex paleobiological changes that took place during the early Danian, and their potential relationship with the Deccan volcanism and the Dan-C2 event, we carried out a detailed analysis of the first ~750 kyr of the Danian at the Caravaca section (SE Spain, western Tethys). We took a multi-proxy approach: quantitative, diversity, taphonomic (fragmentation index) and teratological (percentage of aberrant specimens) analyses of planktic foraminifera, as well as bulk geochemical (stable C- and O-isotopes, $CaCO_3$ content) and magnetic susceptibility measurements. Caravaca is a well-known section for its excellent

exposure, completeness and continuity (Smit, 1982, 2004; Molina et al., 2009), and provides an exceptional opportunity to evaluate paleoclimatic, paleoceanographic and paleobiological changes during the early Danian.

2. Material and methods

We revisited the Caravaca section, which is located in the Barranco del Gredero (38º04'36" N, 1º52'42" W), southwest of Caravaca de la Cruz, SE Spain (Fig. 1). The Danian part of this section consists mostly of hemipelagic marly limestones (Fig. 2), although it starts with the well-known K-PgB clay bed (Smit, 1982, 2004), consisting of a 1-2 mm-thick red air-fall layer and a 6 cm-thick dark clay bed, that is almost black in the lowermost 1.5 cm (Fig. 1E). This section was chosen as an auxiliary section of the Global Boundary Stratotype Section and Point (GSSP) for the base of the Danian Stage (Molina et al., 2009), as it represents one of the most continuous and complete K-PgB sections worldwide (Smit and Hertogen, 1980; Smit and Romein, 1985). Previous studies have focused on the K-PgB clay bed and the first one or two meters of the lowermost Danian, with a significantly lower resolution above this interval (Smit, 1982, 2004; Canudo et al., 1991; Coccioni and Galeotti, 1994; Kaiho and Lamolda, 1999; Arz et al., 2000; Lamolda et al., 2005; Vellekoop et al., 2018; Sepúlveda et al., 2019). In contrast, we sampled the first 820 cm of the Danian at high resolution, taking samples every 1-5 cm over the first 200 cm, and every 25-30 cm across the rest of the section.

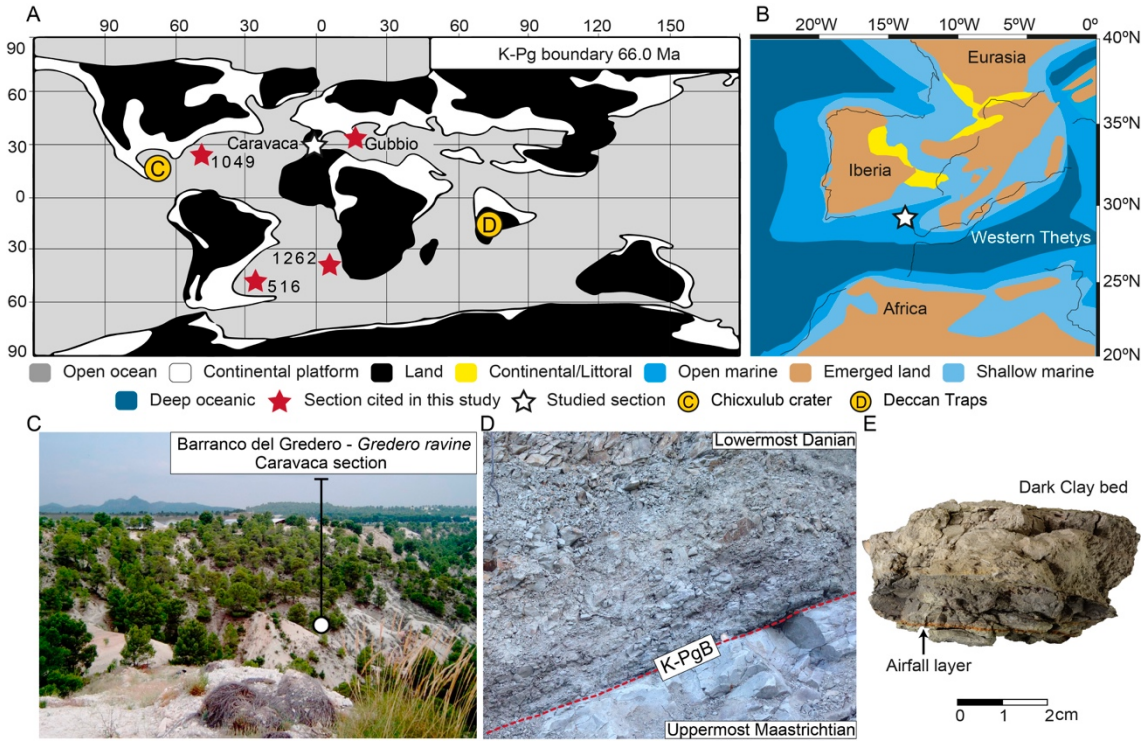

Fig. 1. A) Paleogeographical location map of Caravaca and other localities worldwide: DSDP Site 516, ODP Sites 1262 and 1049, and Gubbio (Contessa Highway section). B) Detailed paleogeographical map of the Western Tethys, with the star indicating the position of Caravaca (modified from Andeweg, 2002). C) Caravaca section overview. D) Detail of the Cretaceous-Paleogene transition. E) Rock fragment of the first 3 centimeters of the K-PgB clay bed at Caravaca, which includes the 1-2 mm thick ejecta-rich air-fall layer and the basal part of dark clay bed.

2.1. Micropaleontological methods

For micropaleontological analyses, a total of 46 samples were disaggregated in H_2O_2 for 3-4 hours. These samples were washed and sieved under running water; the size fraction >63 microns was collected, and the residue was oven-dried at 50 °C for 24 h. Representative splits of ca. 300 individuals per sample were studied for quantitative analyses, classifying the specimens at species level. Representative specimens from Caravaca were photographed with a JEOL JSM 6400 SEM (scanning electron microscope) at the Microscopy Service of the Universidad de Zaragoza (Spain).

For the Danian, we have used the planktic foraminiferal zonation of Arenillas et al. (2004), which was updated by Metsana-Oussaid et al. (2019). In Fig. 2, this biozonation has been compared with the more standardized zonation of Berggren and Pearson (2005), which was revised by Wade et al. (2011). Although the taxonomy used by the authors differs, the close correspondence of biozones and subbiozones is illustrated in Fig. 2. The stratigraphic distribution of Danian planktic foraminiferal species across the Caravaca section is also illustrated in Fig. 2. SEM photographs of index-species and other relevant Danian species are displayed in Fig. 3.

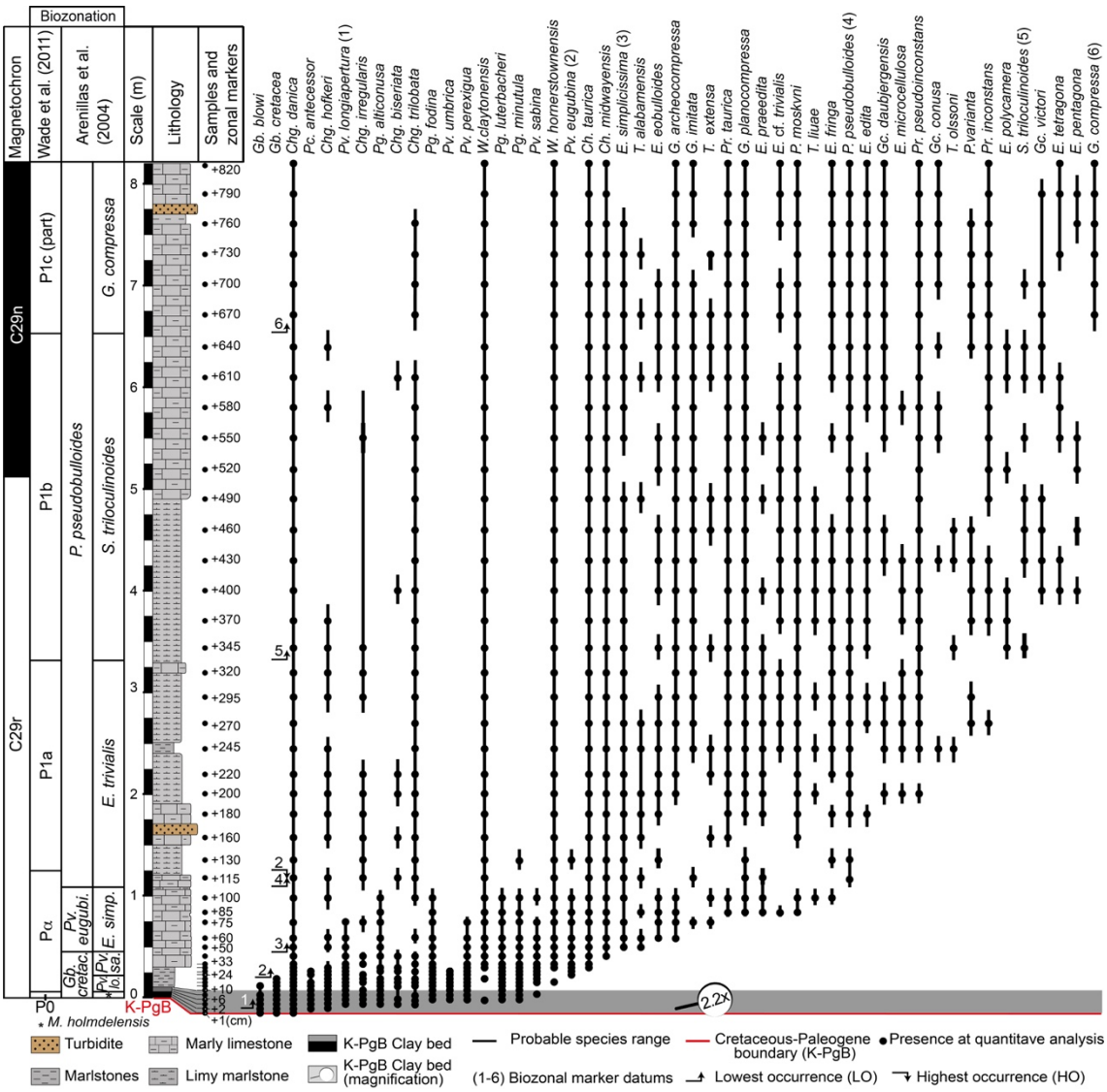

Fig. 2. Stratigraphic column and distribution of the Danian species at Caravaca. *Gb. = Guembelitria; Chg.= Chiloguembelitria; Pc. = Pseudocaucasina; Pg. Palaeoglobigerina; Pv.= Parvularugoglobigerina; W.= Woodringina; Ch. = Chiloguembelina; E.= Eoglobigerina; T.= Trochoguembelitria; G.= Globanomalina; P.= Parasubbotina; Pr.= Praemurica; Gc.= Globoconusa; S.= Subbotina.*

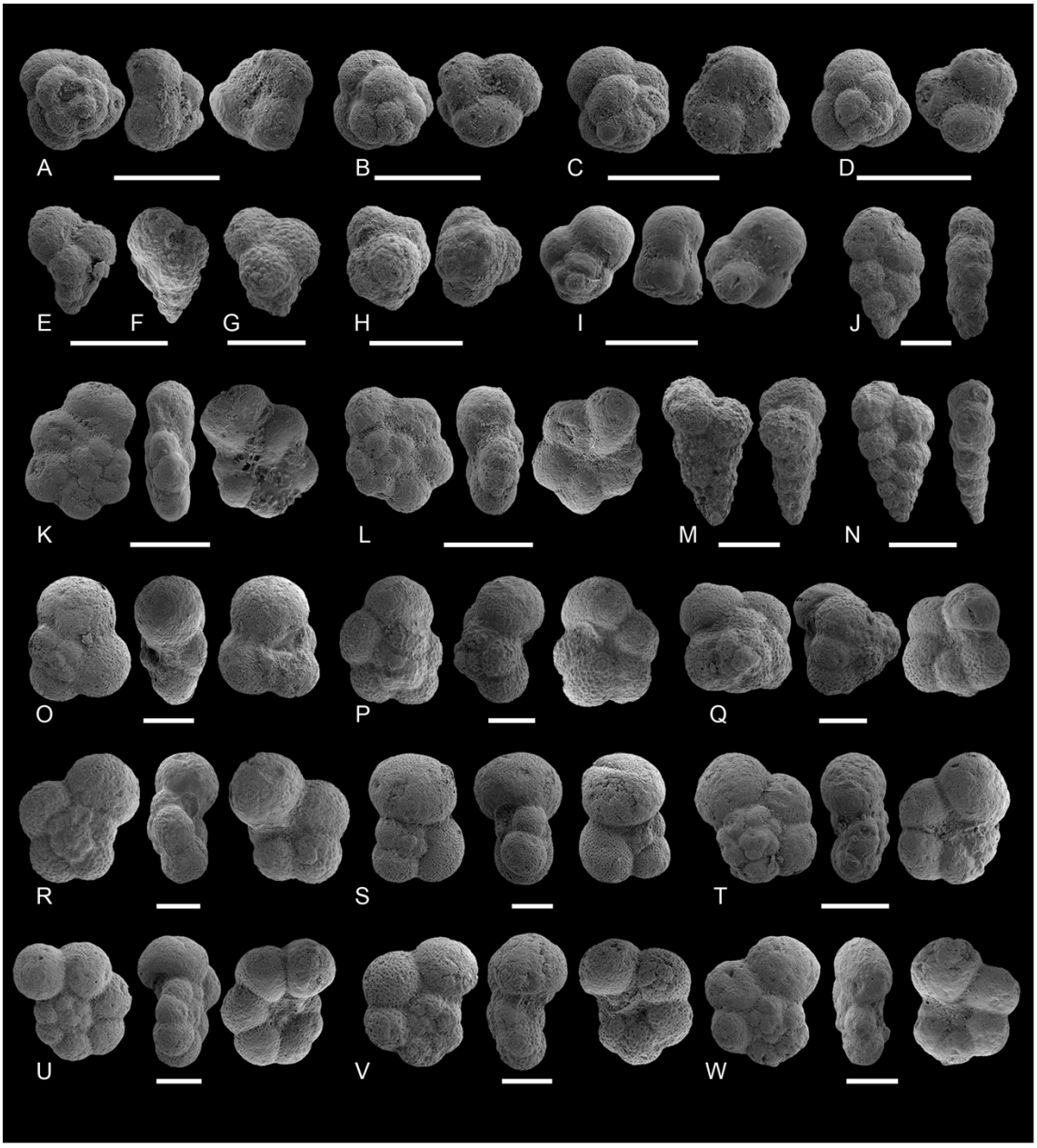

Fig. 3. SEM photographs of *Pseudocaucasina antecessor* (A-D); *Guembelitria cretacea* (E); *Chiloguembelitria hofkeri* (F); *Chiloguembelitria danica* (G); *Trochoguembelitria alabamensis* (H); *Palaeoglobigerina alticonusa* (I); *Chiloguembelina midwayensis* (J); *Parvularugoglobigerina*

longiapertura (K); *Parvularugoglobigerina eugubina* (L); *Woodringina hornerstownensis* (M); *Chiloguembelina taurica* (N); *Eoglobigerina simplicissima* (O); *Eoglobigerina edita* (P); *Eoglobigerina pentagona* (Q); *Parasubbotina pseudobulloides* (R); *Subbotina triloculinoides* (S); *Globanomalina archeocompressa* (T); *Praemurica taurica* (U); *Praemurica inconstans* (V); *Globanomalina compressa* (W). White bar scales = 100 microns.

To identify the planktic foraminiferal acme-stages (PFAS) proposed by Arenillas et al. (2006) for the lower Danian, we used quantitative data (Tables S1, S2) and the PAST software (v4.0.3, Hammer et al., 2001) for R-mode cluster analyses using the well-known Bray-Curtis index. We chose The Bray-Curtis similarity index since it is a more appropriate index for abundance data (i.e. species assemblages) than other distance measures, such as the common Euclidian distance (Beals, 1984; Ricotta and Podani, 2017). The Euclidean distance can lead to misleading results when species abundance data contains zeros (i.e. absences of certain taxa) as this method places more weight on the abundance differences between samples than on the similarities in the assemblage of species (Legendre and Gallagher, 2001). In contrast, in the Bray-Curtis index common and scarce species have relatively similar weights, which means that the assemblage (as opposed to the absolute abundances) becomes the more significant control on distance (Ricotta and Podani, 2017). The criteria for distinguishing the boundaries between PFAS are clear: PFAS-1 is characterized by a dominance of triserial guembelitriids (*Guembelitria*), PFAS-2 by the tiny trochospiral parvularugoglobigerinids (*Parvularugoglobigerina* and *Palaeoglobigerina*), and PFAS-3 by biserial *Woodringina* and *Chiloguembelina*. All three acme-stages, first recognized in the Spanish sections of Zumaia (Arenillas et al., 1998) and Agost (Molina et al., 1998), have been identified in lower Danian sections worldwide (Arenillas et al., 2006, 2016; Gallala et al., 2009; Lowery et al., 2018; Renne et al., 2018).

To reconstruct paleo-environmental change, we have used several planktic foraminiferal proxies: paleoecological preferences of species, the abundance of aberrant specimens, fragmentation index, diversity indices and the planktic/benthic ratio. Early Danian planktic

223 foraminiferal paleoecology has previously been interpreted based on the isotopic signatures of
224 each species (e.g. Olsson et al., 1999; Aze et al., 2011; Birch et al., 2012). In order to discriminate
225 between normal and abnormal specimens, we followed the compendium of aberrant
226 morphologies of Arenillas et al. (2018) for early Danian planktic foraminifera. The fragmentation
227 index (ratio of broken vs. complete foraminifers) was calculated following the method of Berger
228 et al. (1982), and used to identify changes in carbonate preservation state. Benthic foraminifers
229 were picked to evaluate potential dissolution processes by calculating the planktic/benthic (P/B)
230 ratio (% planktic foraminifera of the total number of foraminifera), but they were not
231 taxonomically classified.
232
233 *2.2 Geochemical and geophysical methods.*
234
235 The inorganic and organic carbonate content was measured using duplicate subsamples from
236 70 samples that were weighed into ceramic boats, one of which was roasted in air at 420˚C for 12
237 hours to remove organic carbon. The total carbon content (TC) of the unroasted subsample, and
238 the Total Inorganic Carbon (TIC) of the roasted subsample, were determined using a Strohlein
239 Coulomat 702, in the Department of Earth Sciences of the University of Oxford. The difference
240 between the amount of carbon determined in unroasted and pre-roasted samples provided an
241 estimate of Total Organic Carbon (TOC). Assuming the inorganic carbon content is all associated
242 with $CaCO_3$ allows the estimation of $CaCO_3$ content using the equation from Stax and Stein
243 (1993): $CaCO_3\% = TIC * 8.33$. Reproducibility of %C using this method is typically better than
244 0.1%.
245
246 Measurements of stable carbon and oxygen isotope ratios ($\delta^{13}C$, $\delta^{18}O$) were performed on
247 homogenized bulk powdered sediment from the same 70 samples. Samples were analyzed in the
248 Department of Earth Sciences of the University of Oxford using a GasBench device attached to a
249 ThermoFisher Delta V Advantage gas source isotope ratio mass spectrometer. Oxygen and
250 carbon-isotopes are reported using the standard delta notation ($\delta^{18}O$, $\delta^{13}C$) in parts per mil (‰)

on the Vienna PeeDee Belemnite (VPDB) scale. Calibration of samples to the VPDB scale was achieved using multiple analyses of an in-house standard, NOCZ, which has average values on the VPDB scale of -1.90‰ for $\delta^{18}O$ and 2.18‰ for $\delta^{13}C$. For $\delta^{18}O$, NOCZ has been calibrated to the VPDB scale by comparison with analyses of NBS-19 and NBS-18, which were assigned $\delta^{18}O$ values of -2.20‰ and -23.01‰ respectively. For $\delta^{13}C$, NOCZ has been calibrated to the VPDB scale by comparison with analyses of NBS-19, which was assigned a value of 1.95‰. Repeated analyses of in-house standards suggest a reproducibility ($\pm 1\sigma$) of <0.1 for both $\delta^{13}C$ and $\delta^{18}O$.

The magnetic susceptibility (MS) of 70 samples was measured at the University of Zaragoza, Spain, with a Spinning Specimen Magnetic Susceptibility Anisotropy Meter KLY-35 Kappabridge. Samples were crushed in an agate mortar and measured in cylindrical plastic boxes of 10 cm^3 in volume. MS values are reported relative to mass (m^3/kg).

3. Results

3.1. Biostratigraphy and age model

At the Caravaca section, a total of 49 species and 14 genera of Danian planktic foraminifera (including species of the genus *Guembelitria*) have been identified. Relative abundances of each species are shown in the Supplementary Table 1. Seven subbiozones have been identified: *Mh. holmdelensis* and *Pv. longiapertura* Subzones (of the *G. cretacea* Zone), *Pv. sabina* and *E. simplicissima* Subzones (of the *Pv. eugubina* Zone), and *E.* cf. *trivialis*, *S. triloculinoides* and *G. compressa* (part) Subzones (of the *P. pseudobulloides* Zone). The stratigraphic interval studied corresponds to Pα, P1a, P1b and (part of) P1c of Berggren and Pearson (2005) and Wade et al. (2011). At Caravaca, the bases of these subbiozones are at 0, 3, 22, 42, 107, 332 and 655 cm, respectively, above the K-PgB (Fig. 2).

To establish the age model at the Caravaca section, we linearly interpolated between the K-PgB, the top of the K-PgB dark clay bed, the C29r/C29n magnetic reversal and the C29n/C28r magnetic reversal. Based on the $^{40}Ar/^{39}Ar$ calibrations of Sprain et al. (2018), we have assigned an age of 66.052 Ma to the K-PgB, 65.724 Ma to the C29r/C29n reversal and 65.075 Ma to the C29n/C28r reversal. Based on cosmic ^{3}He sedimentation rates, Mukhopadhyay et al. (2001) estimated a duration for deposition of the K-PgB dark clay bed of ~10 kyr. At Caravaca, the top of the K-PgB dark clay bed is ~6 cm above the K-PgB, and, according to Smit (1982) and Groot et al. (1989), the C29r/C29n and C29n/C28r reversals are at 5.1 m and 9.8 m above the K-PgB respectively. Consequently, the average sedimentation rates at Caravaca are ~0.6 cm/kyr for the K-PgB dark clay bed, 1.58 cm/kyr for the Danian part of C29r and 0.72 cm/kyr for C29n. In total, the studied section spans approximately the first 760 kyr of the Danian. According to this age model, the bases of *Mh. holmdelensis*, *Pv. longiapertura*, *Pv. sabina, E. simplicissima*, *E.* cf. *trivialis*, *S. triloculinoides* and *G. compressa* Subzones occurred at 0, 5, 20, 33, 75, 219, and 528 kyr after the K-PgB, respectively. It is remarkable that *Pseudocaucasina antecessor* (Arenillas and Arz, 2017) has been identified at Caravaca for the first time. Its Lowest Occurrence Data (LOD) is at 1.5 cm above the K-PgB, i.e. 2.5 kyr after the K-PgB. The LODs of its most direct evolutionary descendants, *Parvularugoglobigerina longiapertura* and *Palaeoglobigerina alticonusa*, are at 3 cm above the K-PgB, i.e. 5 kyr after the K-PgB.

3.2. Acme-stratigraphy

Planktic foraminiferal assemblages identified in the lower Danian of the Caravaca section are characterized by low diversities and high consecutive dominances of single taxon groups, corresponding to the succession of the three acme-stages PFAS of Arenillas et al. (2006). This is confirmed by the cluster analysis performed here (Fig. 4).

PFAS-1 spans the first 5 cm of the lower Danian of the Caravaca section (from the K-PgB to the lowermost part of *Pv. longiapertura* Subzone), i.e. the first 8 kyr after the K-PgB boundary

306 according to our age model. PFAS-1 is dominated by triserial taxa, mainly *Guembelitria* and, to
307 a lesser extent, its descendant *Chiloguembelitria. Guembelitria* is the only Cretaceous genus that
308 increased its abundance after the K-PgB. In addition, we have identified a bloom of
309 *Pseudocaucasina antecessor*, which starts within the PFAS-1 and ends at the lowermost part of
310 PFAS-2. (Fig. 5, Table S1).
311
312 PFAS-2 is placed at 5 to 55 cm above the K-PgB at Caravaca (from the lowermost part of
313 *Pv. longiapertura* Subzone to the middle part of the *E. simplicissima* Subzone), i.e. between 8
314 and 41 kyr after the K-PgB. This acme-stage is dominated by parvularugoglobigerinids, i.e.
315 *Parvularugoglobigerina* and *Palaeoglobigerina* (the first evolutionary radiation of Danian
316 species), comprising between 50 and 80% of the assemblages. The LODs of *Woodringina* and
317 *Chiloguembelina*, the first Danian biserial taxa, occurred within PFAS-2, but their combined
318 relative abundance never exceeds 3% except for the upper part of PFAS-2. Around 38 cm above
319 the K-PgB (upper part of the *Pv. sabina* Subzone), biserial taxa show a sharp increase, but they
320 do not exceed the parvularugoglobigerinids in abundance.
321
322 PFAS-3 has been recognized from 55 cm above the K-PgB to the top of the studied section
323 (from the lower part of the *E. simplicissima* Subzone to the lower part of the *G. compressa*
324 Subzone), i.e. between 41 kyr and at least 756 kyr after the K-PgB. The planktic foraminiferal
325 assemblages in PFAS-3 comprise mostly biserial taxa, i.e. the genera *Woodringina* and
326 *Chiloguembelina*, and especially the species *Woodringina hornerstownensis* (30.7% on average).
327 Although PFAS-3 assemblages are dominated by biserial taxa throughout, several substages can
328 be identified on the basis of changes in relative abundances of some other taxa. One of the most
329 striking features within PFAS-3 at Caravaca is the occurrence of three successive blooms of the
330 opportunist triserial *Chiloguembelitria* reaching maxima abundances of 48.5, 28.6, and 12.3%
331 respectively. These *Chiloguembelitria* blooms are successively less intense and alternate in time
332 with remarkable increases in the combined abundance of genera resulting from the second Danian
333 evolutionary radiation, including *Eoglobigerina*, *Parasubbotina*, *Globanomalina*, *Praemurica*,

and *Subbotina,* or "other genera" for short. The latter group reaches maxima abundance values of 43.1, 49.5 and 48.4% between each *Chiloguembelitria* bloom (Fig. 5). Cluster analyses strongly support the further division of PFAS-3 into 7 shorter substages following the alternation of major groups (Fig. 4), with each substage named as PFAS-3 plus a suffix: α, T1, O1, T2, O2, T3, O3. Stratigraphic and temporal boundaries of each stage and substage, with average relative abundances of major groups are listed in Table 1.

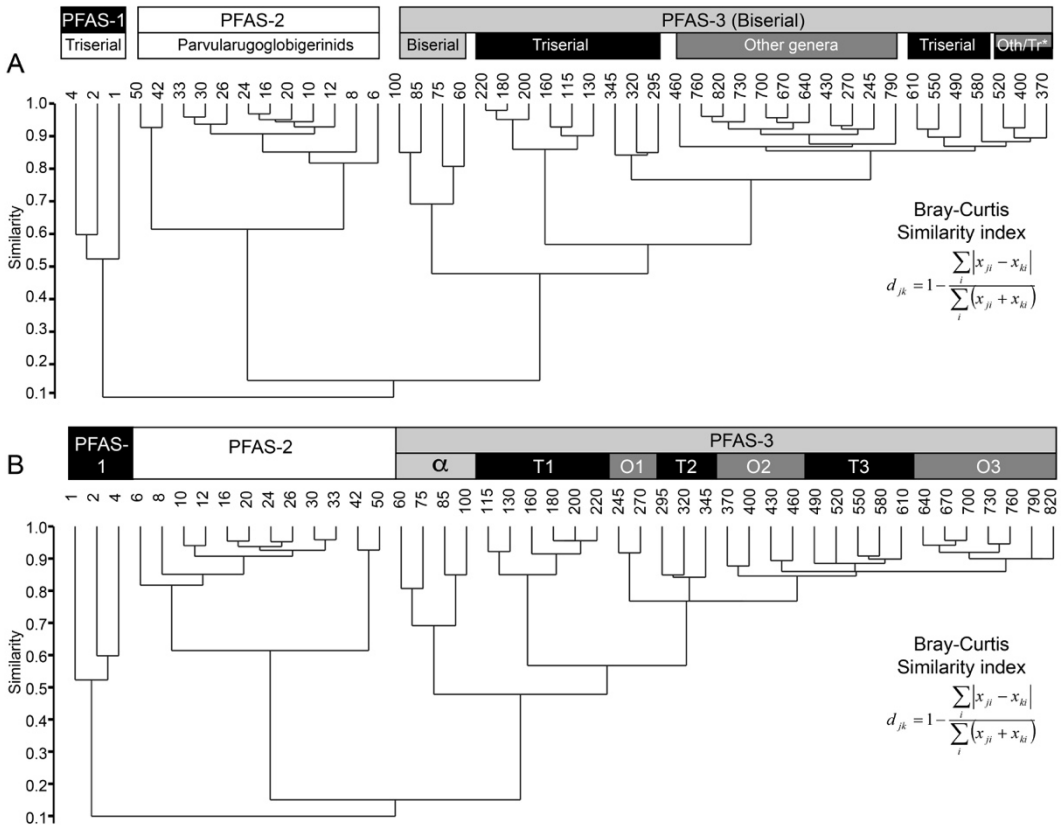

Fig. 4. A) Agglomerative clustering based on the unweighted paired group method with the arithmetic mean (UPGMA) and the Bray-Curtis similarity index. Oth/Tr*. = Clusters with ambivalent affinity. B) Stratigraphically constrained dendrogram.

Table 1. Stratigraphic height and age of PFAS and relative abundance of major groups

PFAS	Height from K-PgB (cm)		Age from K-PgB (kyr)		Major groups relative abundance (%)			
	Base	Top	Base	Top	Triserial	Parvul.	Biserial	Others

PFAS-3O3	625	820*	487	756*	2.3%	0.0%	56.9%	40.8%
PFAS-3T3	475	625	311	487	8.8%	0.0%	59.5%	31.7%
PFAS-3O2	357	475	235	311	6.6%	0.0%	53.6%	39.8%
PFAS-3T2	282	357	187	235	21.4%	0.0%	58.8%	19.8%
PFAS-3O1	232	282	155	187	2.4%	0.0%	55.6%	41.9%
PFAS-3T1	107	232	75	155	45.2%	0.0%	49.0%	5.8%
PFAS-3α	55	107	41	75	0.8%	24.7%	67.0%	7.5%
PFAS-2	5	55	8.3	41	9.7%	83.4%	6.8%	0.1%
PFAS-1	K-PgB	5	0	8.3	76.1%	23.1%	0.9%	0.0%

Table 1. Stratigraphic position and calibrated age of planktic foraminiferal acme-stages (PFAS) at Caravaca, and relative abundances of the major planktic foraminiferal groups. * = Top of the studied section. Parvul.=Parvularugoglobigerinids

PFAS-3α is characterized almost exclusively by biserial *Woodringina* and *Chiloguembelina,* but mostly by *Woodringina* (Fig. 5). The LODs of *Eoglobigerina*, *Parasubbotina*, *Globanomalina*, *Praemurica* and *Trochoguembelitria* are at 55-85 cm above the K-PgB, forming the second evolutionary radiation of Danian species (Fig. 2 and Fig. 5). The Highest Occurrence Data (HOD) of *Palaeoglobigerina* and *Parvularugoglobigerina* are recognized towards the top of PFAS-3α, as these species were completely replaced by the incoming species of the second Danian evolutionary radiation.

PFAS-3T (1-3) are characterized by subsequent blooms of triserial *Chiloguembelitria*. PFAS-3T1 witnessed the LOD of the genus *Globoconusa*, which occupies the same ecological niche as *Guembelitria* and *Chiloguembelitria* (see Olsson et al., 1999), although during each *Chiloguembelitria* bloom the relative abundance of *Globoconusa* remains extremely low with values <1% (0.1, 0.2, and 0.9%).

PFAS-3O (1-3) refers to the substages characterized by the higher relative abundance of the "other genera" combination. The genera *Globanomalina* (15.2%) and *Praemurica* (9.9%) are the

most abundant genera during each PFAS-3O. It is noteworthy that the alternations between PFAS-3T and PFAS-3O occurred rapidly, especially between the first three alternations: T1-O1, O1-T2, and T2-O2 (Fig. 5 and Tables 1, 2).

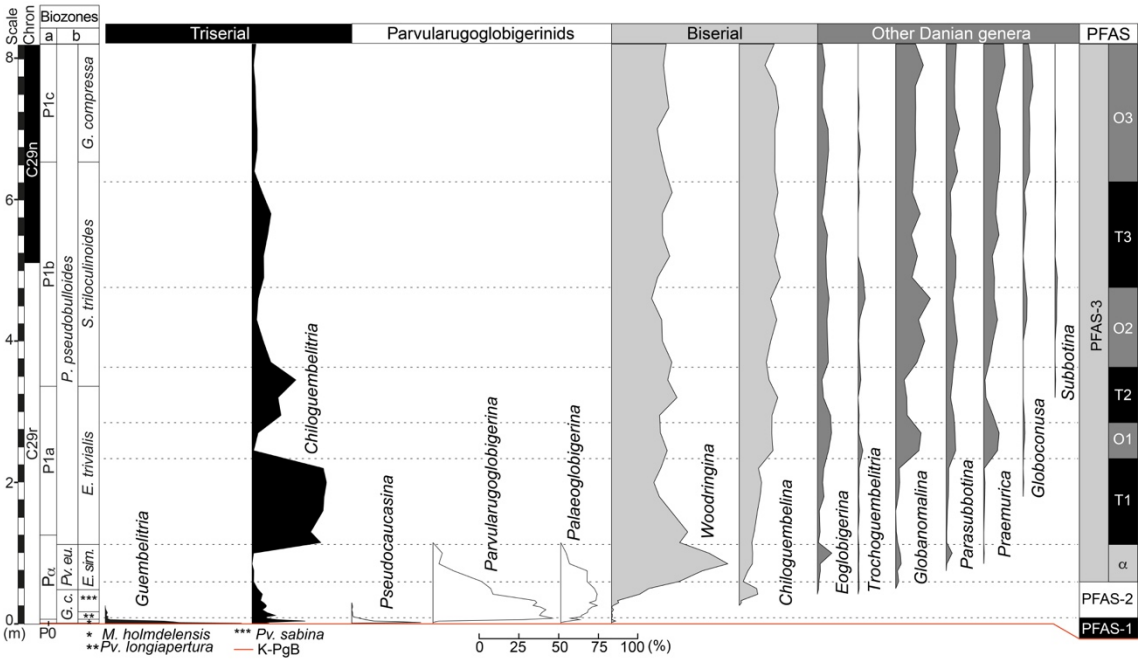

Fig. 5. Relative abundance of the Danian planktic foraminiferal genera and major groups at Caravaca. Biozones: a = (Wade et al., 2011); b = (Arenillas et al., 2004).

3.3. Diversity indices.

Standard diversity indices are summarized in Table 2 and shown in full in Table S2. We have calculated the average diversity values for PFAS-1-2 and for each substage of PFAS-3. The diversity indices provide evidence for rapid and abrupt environmental changes from PFAS-1 to the end of PFAS-3T1 (suggesting less resilient planktic foraminiferal assemblages), and more stable environmental conditions from PFAS-3O1 onwards (suggesting more resilient assemblages). However, it is noteworthy that the rapid evolutionary radiations which occurred during the PFAS-2 and PFAS-3α intervals (Figs. 2 and Fig. 5) highly influenced the values of the diversity indices. Conversely, from the base of PFAS-3O1 to the top of the section, diversity

386 indices show more gradual changes, showing slightly higher average diversity values in PFAS-
387 3O substages than in the PFAS-3T substages (see Table 2).
388
389

Table 2. Diversity indices and relative abundance of aberrant forms of major groups in each PFAS

PFAS	Main diversity indices				Relative abundance of aberrant forms (%)				
	S	H´	1/λ	E	Triserial	Parvul.	Biserial	Others	Total
PFAS-3O3	23	2.42	6.86	0.48	0.0%	0.0%	1.3%	1.3%	2.6%
PFAS-3T3	23	2.37	6.91	0.47	0.4%	0.0%	1.9%	1.4%	3.7%
PFAS-3O2	26	2.55	8.09	0.49	0.2%	0.0%	2.2%	1.7%	4.1%
PFAS-3T2	24	2.31	6.60	0.42	2.8%	0.0%	5.1%	2.2%	10.0%
PFAS-3O1	25	2.54	8.46	0.52	0.2%	0.0%	2.9%	2.4%	5.5%
PFAS-3T1	18	1.95	4.86	0.41	6.9%	0.0%	5.1%	0.5%	12.5%
PFAS-3α	20	1.88	4.24	0.33	0.0%	1.3%	4.6%	0.7%	6.6%
PFAS-2	15	1.71	3.95	0.40	1.0%	9.0%	0.7%	0.7%	11.5%
PFAS-1	6	1.26	3.13	0.64	17.3%	3.7%	0.0%	0.0%	21.0%

390
391 Table 2. Average values of main diversity indices for each planktic foraminiferal acme-stage (PFAS), and
392 relative abundance of the aberrant forms in total, and in each major group. S = Species richness; H '=
393 Shanon-Weaver index; 1/λ.= Inverse Simpson index; E = Evenness; Parvul. = Parvularugoglobigerinids
394
395 *3.4. Aberrant index*
396
397 We have found abnormal specimens of *Guembelitria* and almost every incoming Danian
398 species (Supplementary Table S3), whereas reworked Cretaceous specimens within Danian
399 sediments display almost no aberrations. According to the terminology of Arenillas et al. (2018),
400 the most common aberrant morphologies identified at Caravaca are: 1) chamber abnormalities:
401 aberrant chamber shapes, reduced chamber sizes and overdeveloped chamber sizes; 2) an
402 abnormal ultimate chamber: aberrant shape, anomalous position and bulla-like chamber; 3)

multiple ultimate chambers: double or twinned ultimate chambers, and a proliferation of chambers; 4) distortion in test coiling; 5) abnormal tests. Some examples of these aberrations are illustrated in Fig. 6. The aberrant forms of planktic foraminifera are mainly abundant within the first 357 cm (~230 kyr) of the Danian (i.e. from the K-PgB to the top of PFAS-3T2), close to the base of the *S. triloculinoides* Subzone (Fig. 7).

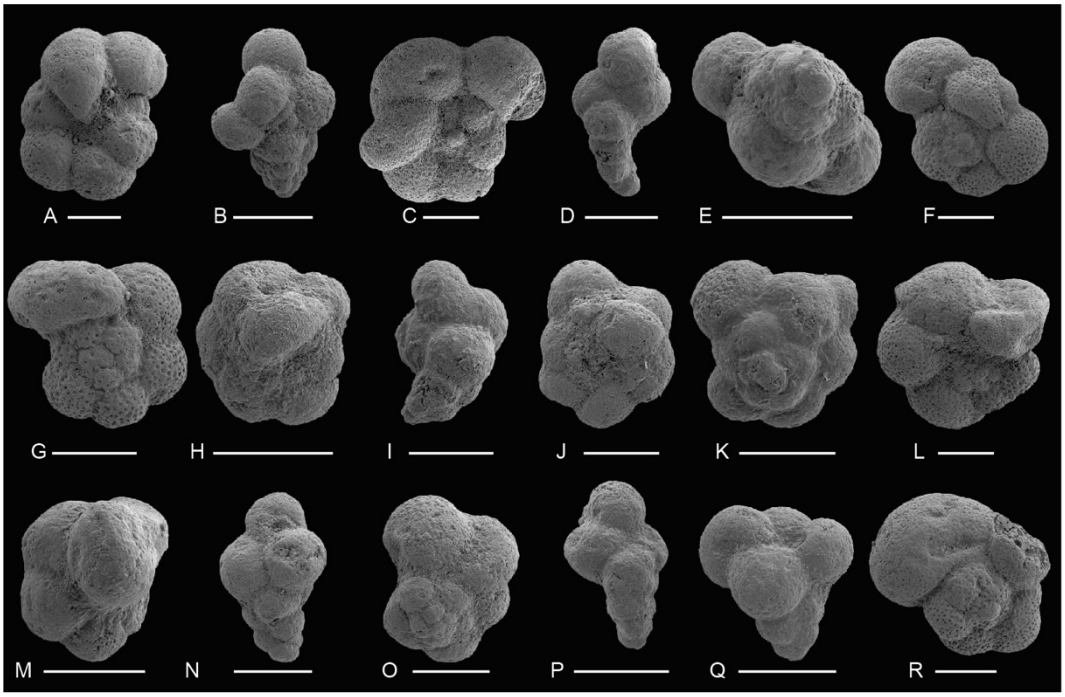

Fig. 6. Examples of different aberrant morphologies within the studied specimens; (A) overdeveloped chamber size; (B) protuberant chamber; (C) aberrant shape; (D) overdeveloped chamber size + anomalous position; (E) proliferation of chambers; (F) aberrant chamber shape; (G) abnormal ultimate chamber; (H) bulla-like chamber; (I) distortion in test coiling and reduced ultimate chamber size; (J) additional chamber; (K) abnormal test; (L) abnormal ultimate chamber; (M) bulla-like chamber; (N) chamber in anomalous position; (O) abnormal test; (P) ultimate chambers in anomalous position and distortion in test coiling; (Q) proliferation of chambers; (R) overdeveloped ultimate chamber with aberrant shape.

PFAS-1 and PFAS-2 are characterized by high relative abundances of aberrant specimens (Fig. 7 and Table 2). The species most commonly displaying aberrant forms are either *G. cretacea* (14.4%) or *Ps. antecessor* (3.5%) for PFAS-1, and *Pv. longiapertura* (5.8%) for PFAS-2. The

aberrant specimens of PFAS-3α mainly belong to biserial taxa, especially to *Woodringina hornerstownensis* (3.1%). The average aberrant index during PFAS-3α (6.6%) is significantly lower than during PFAS-2 (11.5%), while during PFAS-3T1 it reaches 12.5%, which is similar to that reached previously in PFAS-2. Triserial and biserial aberrant forms are dominant during PFAS-3T substages, especially for *Chg. danica* and *W. hornerstownensis* species. During PFAS3-T1, T2 and T3, aberrant forms of *Chg. danica* represent, respectively, 5.2, 1.6 and 0.3% on average of total planktic foraminiferal specimens, and 3.3, 2.5 and 1.0% for *W. hornerstownensis*. Each triserial bloom, i.e. PFAS-1, PFAS-3T1, PFAS3-T2 and to lesser extent PFAS3-T3, displays a transient increase of the aberrant index (Fig 7 and Table 2). Conversely, during the blooming episodes of the "other genera", i.e. PFAS-3O1, PFAS-3O2 and PFAS-3O3, there are fewer aberrant specimens. The most common biserial species with aberrant forms within PFAS-3O substages are *W. hornerstownensis* with respectively 1.8, 1.2 and 0.8% on average, and the most common aberrant specimens of the "other genera" belong to the species *Globanomalina archeocompressa* (0.55%) for PFAS3-O1, *Praemurica taurica* (0.4%) for PFAS3-O2 and *Pr. inconstans* (0.3%) for PFAS3-O3.

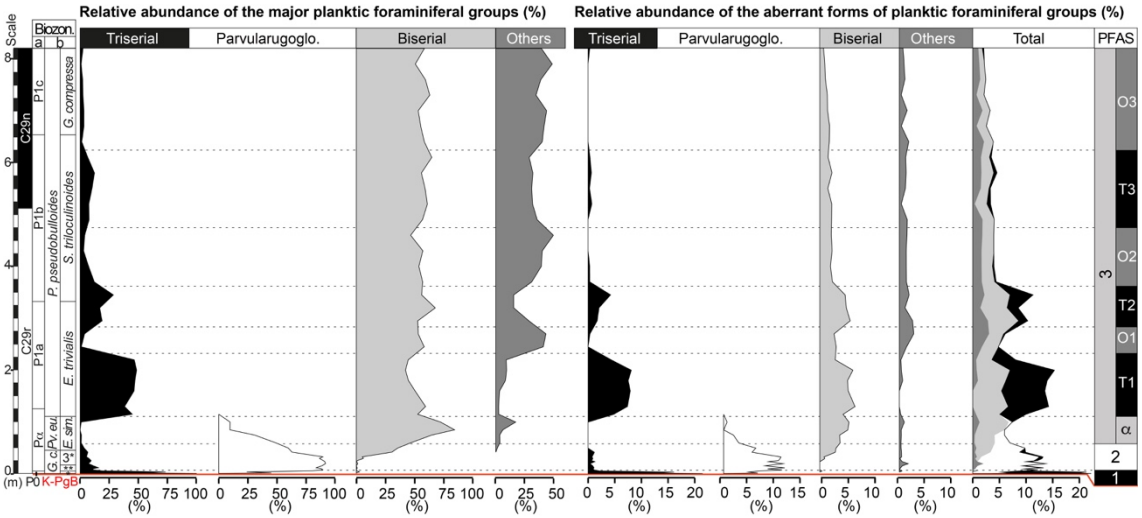

Fig. 7. Comparison of the quantitative results for the major groups of planktic foraminifera. Parvularugoglo. = parvularugoglobigerinids.

3.6. Carbonate preservation and magnetic susceptibility

443

444 At Caravaca, the $CaCO_3$ content ranges from 15.5 to 88.4 % with a mean value of 73.78%
445 (n = 70). The lowest $CaCO_3$ content has been identified in the K-PgB clay bed (0-6 cm, between
446 15.53 and 39.7%, and 28% on average). From 6 to 26 cm above the K-PgB, the $CaCO_3$ content
447 increases sharply to 70%, and from 26 to 115 cm the average $CaCO_3$ content is 83%. There is a
448 decrease in the average $CaCO_3$ content from 115 to 520 cm above the K-PgB (71%) with two
449 relatively low values identified at 245 (60.5%) and 430 (65.5%) cm above the K-PgB (Fig. 8C).
450 Finally, from 520 cm to the top of section, the average $CaCO_3$ content is relatively stable at 80%
451 on average.

452

453 Apparent dissolution features on tests, such as abrasion marks, broken and/or isolated
454 chambers, or corroded walls, have been identified, but they are not abundant. The planktic
455 foraminiferal preservation is moderate to good in most of the samples, with the exception of those
456 from the dark K-PgB clay bed. We consider that samples with planktic foraminiferal
457 fragmentation ratio or fragmentation index (FI) >40% represent intervals of strong dissolution
458 (e.g., Kucera et al., 1997; Gilabert et al., 2021). Values of planktic foraminiferal fragmentation
459 vary between 7 and 45% across the Caravaca section, with an average fragmentation of 18.3% (n
460 = 46). The average fragmentation values are high (45%) in the K-PgB dark clay bed, moderate
461 (20%) between 6 and 520 cm, and low (13%) from 520 cm to the top of the section (Fig. 8D).

462

463 At Caravaca, the P/B ratio (Fig. 8F) ranges between 11 and 100%, with three distinct
464 intervals: in the dark K-PgB clay bed P/B ratios range between 11 and 47%; from 6 to 26 cm
465 above the K-PgB, they are between 72 and 89%; and from 30 cm to the top of the studied section,
466 they are between 95 and 100%. Benthic foraminifera are more resistant to fragmentation and
467 dissolution than planktic foraminifera, and the P/B ratio is expected to decrease with increasing
468 dissolution intensity (Kucera et al., 1997). The significant, negative correlation $r = -0.75$ $p < 0.01$
469 between FI and the P/B suggests that higher dissolution of planktic foraminifera is related to lower
470 P/B values, which are limited to the K-PgB clay bed.

Magnetic susceptibility (MS) oscillates between $1.67x10^{-8}$ and $1.23x10^{-7}$ m^3/kg across the Caravaca section, with a mean value of $3.51x10^{-8}$ m^3/kg. MS values are within the standard range of values for lithified marine samples containing typical paramagnetic minerals (Ellwood et al., 2008). MS values increase between 115 and 520 cm above the K-PgB, with maxima at 245 and 430 cm, mirroring the $CaCO_3$ curve (Figs. 8C and 8E). The strong negative correlation between MS and $CaCO_3$ content suggests variations in the original detrital influx or variations in the flux of carbonate, causing variations in the concentration of paramagnetic minerals.

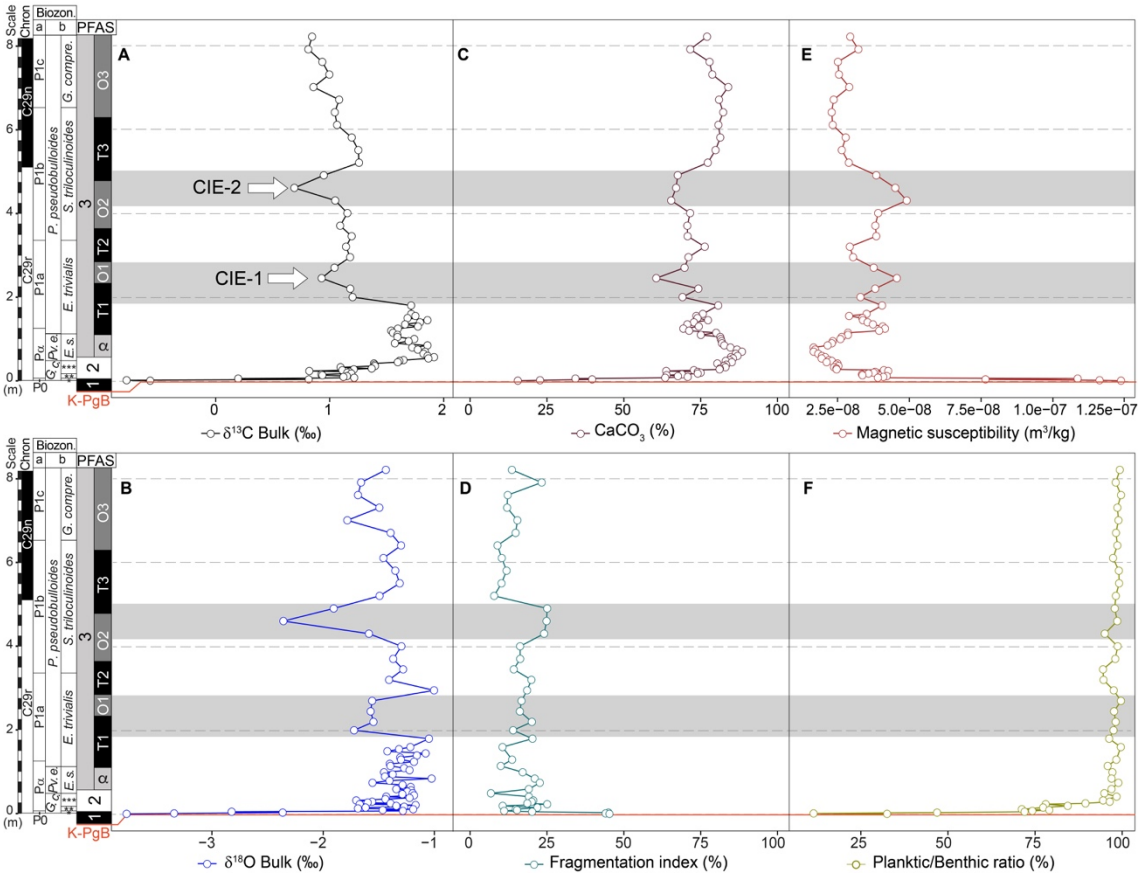

Fig. 8. A-B) Stable isotopes; C) Carbonate content; D) Fragmentation index; E) Magnetic susceptibility; and F) Planktic/Benthic ratio at Caravaca. Data can be found in Supplementary Table 4.

3.7. Stable isotopes (bulk carbonate $\delta^{13}C$ and $\delta^{18}O$)

At Caravaca, $\delta^{13}C$ and $\delta^{18}O$ values for bulk carbonate show a moderate degree of correlation ($r = 0.62$, $p < 0.01$) and evolve in parallel in some intervals. However, values are comparable with those previously reported for the lower Danian at the Caravaca section (Kaiho et al., 1999; Sosa-Montes de Oca et al., 2016; Sepúlveda et al., 2019) and other sections worldwide (see compilation in Hull et al., 2020), suggesting little influence of diagenesis. Only in the K-PgB clay bed do $\%CaCO_3$ and stable isotope values exhibit a significant correlation. In the rest of the studied section, the correlation between $\%CaCO_3$ and $\delta^{18}O$ or $\delta^{13}C$ values is poor to very poor, with $r = 0.54$ ($p < 0.01$) between $\%CaCO_3$ and $\delta^{13}C$, and $r = 0.32$ ($p < 0.01$) between $\%CaCO_3$ and $\delta^{18}O$. This lack of significant correlation suggests that the lithology exerts very little control on the stable isotope values.

The $\delta^{13}C$ values vary between -0.78‰ and +1.92‰ at Caravaca (Fig. 8A) with the lowest $\delta^{13}C$ values registered within the K-PgB dark clay bed, ranging from -0.78‰ to 0.20‰. From 6 to 57 cm above the K-PgB, $\delta^{13}C$ increases to the highest values of the section at ~1.92‰. Between the maximum $\delta^{13}C$ value at 57 cm to 180 cm, $\delta^{13}C$ displays very small oscillations between 1.92 and 1.71‰. From 180 cm to the top of the section, $\delta^{13}C$ broadly displays a clear overarching trend to lower values, with two negative carbon isotopic excursions (CIEs) superimposed upon this trend. The first (CIE-1) has a minimum value of 0.93‰ at 245 cm and the second (CIE-2) a minimum value of 0.69‰, at 460 cm above the K-PgB.

The $\delta^{18}O$ values are broadly invarient across much of the Caravaca section, except for three distinct negative excursions (Fig. 8B), the first at the K-PgB and the other two coinciding approximately with the CIEs described above. $\delta^{18}O$ values are the lowest of the whole section within the K-PgB clay bed ranging from -3.77‰ to -2.82‰. The other two minima in $\delta^{18}O$ occur at 200 cm above the K-PgB (slightly below the CIE-1), and 460 cm, coincident with CIE-2.

4. Recognizing the Dan-C2 event at Caravaca

514 The Dan-C2 event was first recognized in the NW Atlantic (ODP 1049), and SE Atlantic
515 (DSDP 527 and 528) and defined as a pair of major, fairly symmetrical, negative excursions in
516 $\delta^{13}C$ and $\delta^{18}O$ (Fig. 9), associated with decreased carbonate content and increased clay content
517 and magnetic susceptibility values (Quillévéré et al., 2008). At Caravaca, the stratigraphic interval
518 corresponding to Dan-C2, as defined in some Atlantic and Tethyan sections (Fig. 9), is recorded
519 between 200 and 490 cm above the K-PgB, from the middle part of *E.* cf. *trivialis* (P1a) Subzone
520 to the middle part of *S. triloculinoides* (P1b) Subzone, i.e. between 130 and 315 kyr after the K-
521 PgB according to our age model. The CIEs identified in Caravaca (CIE-1 and CIE-2) are within
522 this stratigraphic interval and consequently they are correlated with the two characteristic negative
523 excursions of Dan-C2 defined elsewhere (Quillévéré et al., 2008; Coccioni et al., 2010). Using
524 our age model, the peak minimum values of CIE-1 and CIE-2 occur 158 and 295 kyr, respectively,
525 after the K-PgB and each CIE has a duration of ~40 kyr. In addition, both CIEs are associated
526 with the lowest $CaCO_3$ content and the highest MS values. According to our age model, the entire
527 Dan-C2 event lasted approximately 185 kyr, ending around the C29r/C29n magnetic reversal
528 (Fig. 9 and Fig. 10A). The small discrepancies in the assigned ages of Dan-C2 between Caravaca
529 and elsewhere (Fig. 9) are probably related to differences and uncertainties in the age models
530 and/or variations in the local sedimentation rates between tie points that are not represented by
531 linear interpolation. Nevertheless, all of different records suggest a broadly consistent age for
532 Dan-C2 and a termination of the event near the C29r/C29n reversal.

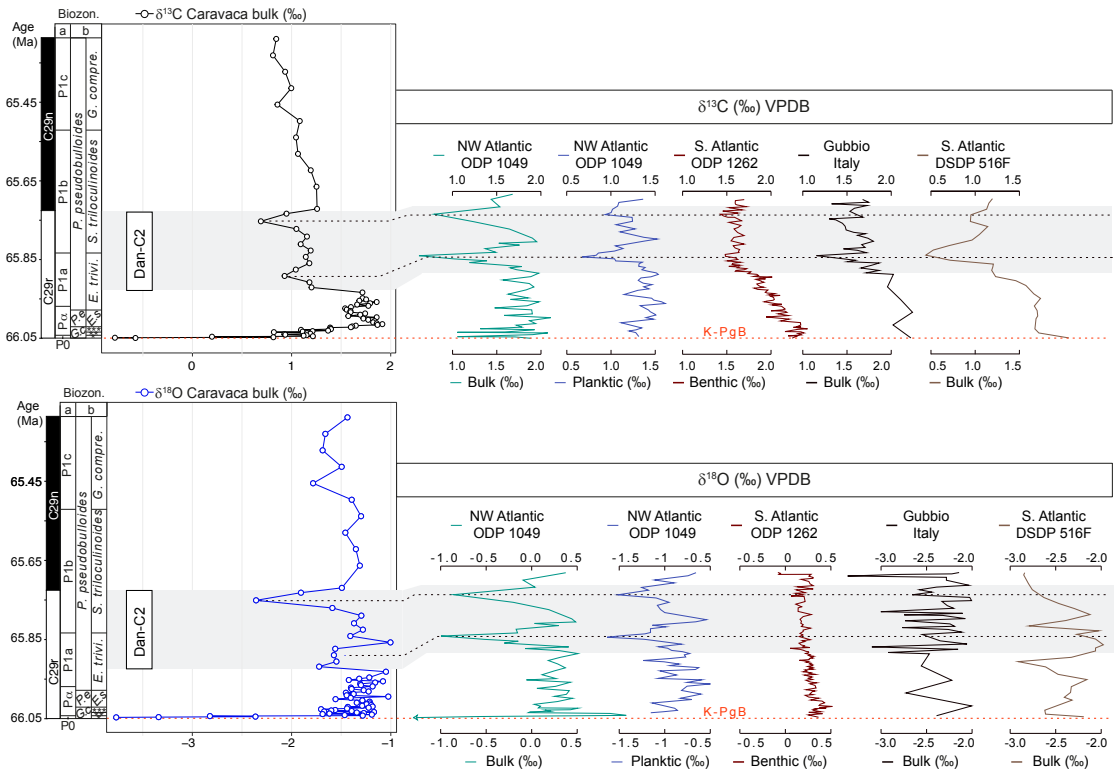

Fig. 9. Worldwide correlation of the Dan-C2 event according to our age model and the $\delta^{13}C$ and $\delta^{18}O$ records from several localities: Caravaca (this report), ODP Site 1049 (Quillévéré et al., 2008), DSDP Site 516 (Krahl et al., 2020), ODP Site 1262 (Barnet et al., 2019), and Contessa Highway (Gubbio) section (Coccioni et al., 2010).

5. Early Danian paleoenvironmental and paleoclimatic evolution

5.1. The K-PgB dark clay bed and PFAS-1 (Guembelitria acme): the aftermath of the Chicxulub impact

Worldwide, the K-PgB dark clay bed was deposited above the Chicxulub-linked air-fall layer under conditions of global climatic warming and alterations in oceanic productivity and acidity (D'Hondt et al. 1998; Coxall et al. 2006; Kawaragi et al., 2009; Birch et al. 2016; Henehan et al., 2016, 2019). At Caravaca, as in most continuous marine sections, the K-PgB dark clay bed is characterized by very low values in $\%CaCO_3$, $\delta^{18}O$ and $\delta^{13}C$ (Figs. 8A, 8B and Figs. 10D, 10E) (see Schulte et al., 2010, and references therein). In addition, the highest planktic foraminiferal

550 fragmentation index values at Caravaca occur within the K-PgB dark clay bed. These geochemical
551 and preservational changes have been directly related to the decimation of pelagic marine
552 calcifiers at the K-PgB (Smit, 1982; Bown, 2005), and subsequent ocean acidification (Alegret et
553 al., 2012; Henehan et al., 2019). At Caravaca, the P/B ratio across the K-PgB dark clay bed is
554 very low, around 30% in comparison to the P/B ratio values-for most of the Danian (Table S2).
555 This decreased P/B ratio is more compatible with the sudden extinction of planktic foraminifera
556 at the K-PgB than with rapid paleobathymetric changes, as previously shown by Alegret et al.
557 (2003). Therefore, the K-PgB dark clay bed records a brief interval of time in which the
558 ecosystems collapsed and the oceans acidified (D´Hondt et al., 1998; Arenillas et al., 2006, 2018;
559 Kring, 2007; Henehan et al., 2019). Biological recovery, however, was relatively quick and
560 oceanic productivity was rapidly re-established after the K-PgB (Sepúlveda et al., 2009, 2019;
561 Lowery et al., 2018; Gibbs et al., 2020). Productivity may have been controlled by blooms in the
562 non-calcareous algal and microbial communities in the open ocean after the K-PgB event, which
563 potentially provided a food supply for higher trophic levels such as calcareous plankton (Bralower
564 et al., 2020).
565
566 The acme of the stress tolerant and opportunistic genus *Guembelitria* during PFAS-1 is
567 recorded within the K-PgB dark clay bed, immediately above the air-fall layer.
568 Contemporaneously, the start of an acme of the opportunist calcareous dinocyst *Thoracosphaera*
569 (Fig. 10B) has been reported above the K-PgB at Caravaca (Lamolda et al., 2005, 2016) and in
570 many other Tethyan sections (Romein, 1977; Smit, 1982; Pospichal, 1996; Gardin, 2002;
571 Lamolda et al., 2005, 2016; Fornaciari et al., 2007; Thibault et al., 2018). The highest planktic
572 foraminiferal aberrant index (21%) of the whole section occurs in PFAS-1 (Fig. 10C); a value
573 which is comparable to other Tethyan and North Pacific localities (Gerstel et al., 1986; Coccioni
574 and Luciani, 2006; Arenillas et al., 2018), suggesting stressed conditions on a global scale.
575 Detrimental environmental effects such as eutrophication, warming, ocean acidification, low
576 oxygenation, and the remobilization of pollutants and toxic heavy metals all occurred potentially
577 in the aftermath of Chicxulub impact and can be attributed to it (Smit, 1999; Coccioni and Luciani,

2006; Ballent and Carignano, 2008; Omaña et al., 2012; Arenillas et al., 2018; Henehan et al., 2019). Nonetheless, a minor contribution by Deccan volcanism to some of these environmental changes cannot be entirely ruled out.

5.2. PFAS-2: recovery and the first radiation of planktic foraminifera

Within PFAS-2, an initial recovery of planktic foraminiferal assemblages and a first evolutionary radiation took place. This first evolutionary radiation was mostly related to the evolution and proliferation of the tiny trochospiral species belonging to *Parvularugoglobigerina* and *Palaeoglobigerina* genera. Recently, Arenillas and Arz (2017) proposed that parvularugoglobigerinids originated from a benthic foraminifer that evolved into a planktic form, such as *Ps. antecessor*. Both *Parvularugoglobigerina* and *Palaeoglobigerina* genera radiated and proliferated during PFAS-2, which, together with the continued dominance of *Thoracosphaera* (Lamolda et al., 2005, 2016) and the very high (11.5%) abundance of aberrant specimens, suggests that conditions remained unstable and stressed throughout PFAS-2.

At Caravaca, a rapid rebound (< 20 kyr) of the carbonate preservation state between PFAS-1 and PFAS-2 is supported by the rapid increase in $\%CaCO_3$ and P/B ratios, and a decrease in the fragmentation index and MS values (Fig. 8). According to Henehan et al. (2016, 2019), the initial surface ocean acidification after the K-PgB, together with the extinction of calcifying organisms, would have led to a transient reduction in the marine alkalinity sink. With the return of marine calcifiers, the excess of alkalinity in seawater was removed leading to a rapid rebound and overshoot in surface ocean pH within 40 kyr after the K-PgB. This process likely explains the rapid increase in $\%CaCO_3$ during PFAS-2. The $\delta^{13}C$ values sharply increase through PFAS-2, returning to relatively stable background values similar to those recorded in the uppermost Maastrichtian of Caravaca (e.g. Kaiho et al.,1999; Sosa-Montes de Oca et al., 2016; Gilabert et al., 2021). This trend in $\delta^{13}C$ also suggests that there was a rapid return of oceanic productivity (Sepúlveda et al., 2019).

606

607 *5.3. Onset of PFAS-3* (PFAS-3α) *and the second radiation of planktic foraminifera*

608

609 The biserial taxa *Woodringina* and *Chiloguembelina* proliferated throughout PFAS-3 but
610 especially during PFAS-3α, when *Woodringina* was the dominant taxon (Fig. 5). A second
611 radiation of Danian planktic foraminifera took place within PFAS-3α with the first appearance of
612 several incoming Danian genera including *Eoglobigerina*, *Globanomalina, Parasubbotina,*
613 *Praemurica* and *Trochoguembelitria*. Most of these new genera seem to have occupied
614 thermocline and subthermocline depths (see Olsson et al., 1999; Aze et al., 2011 and references
615 therein) thus suggesting an initial reoccupation of deeper depth habitats and an incipient but
616 increased water column stratification. The dominance of *Woodringina* during PFAS-3α suggests
617 relatively warm conditions (see Olsson et al., 1999 and references therein) during this stage. A
618 similar bloom of biserial taxa at Gubbio has been interpreted as an overall reduction in
619 oxygenation of the mixed layer in the oceans (Coccioni et al., 2010) similar to conditions during
620 blooms of biserial taxa during the late Maastrichtian (Pardo and Keller, 2008).

621

622 During PFAS-3α, *Thoracosphaera* was still the dominant calcareous nannoplankton genera
623 although *Braarudosphaera* started to replace it as the dominant taxon, at least in the western
624 Tethys (Romein 1977; Smit, 1982; Lamolda et al., 2016). *Braarudosphaera* species are thought
625 to have been abundant in the lower photic zone under low temperature, low salinity, and eutrophic
626 conditions, and therefore *Braarudosphaera* species are typically considered opportunists and are
627 associated with episodes of environmental stress (Bukry, 1974; Cunha and Shimabukuro, 1997;
628 Kelly et al., 2003; Lamolda et al., 2005, 2016; Jones et al., 2019). The appearance of incoming
629 species of planktic foraminifera and nannofossils characteristic of deeper water depth habitats
630 suggests a first step for the recolonization of deeper niches. However, it is well-known that the
631 entire reoccupation of the deeper ocean niches by planktic foraminifera, as well as the rebound of
632 diversity levels comparable to pre-KBP levels, took several million years (Aze et al., 2011; Birch

et al., 2012, 2016; Lowery and Fraas, 2019). Within PFAS-3α, carbonate parameters (%$CaCO_3$ and the fragmentation index) are similar to those in PFAS-2.

5.4. Chiloguembelitria blooms during PFAS-3 and the Dan-C2 event

Triserial guembelitriid blooms like those recorded during PFAS-3T substages are the most common planktic foraminiferal indicators of high environmental stress (Kroon and Nederbragt 1990; Coccioni and Luciani, 2006; Pardo and Keller, 2008; Punekar et al., 2014a,b; Arenillas et al., 2018). In addition, during each triserial bloom identified at Caravaca, a rise in the aberrant index has been identified (Fig. 10B and 10C). Danian triserial guembelitriid blooms have been commonly ascribed to the effect of Deccan volcanism, and linked to the Dan-C2 event (Punekar et al., 2014a; Keller et al., 2016). At Caravaca, the two main *Chiloguembelitria* blooms (PFAS-3T1 and T2) are related to strong increases in the aberrant index (Fig. 7), suggesting higher stress conditions, similar to those reported in Tunisian sections (Arenillas et al., 2018).

A triserial guembelitriid acme, such as the bloom of *Guembelitria* (here *Chiloguembelitria*) during PFAS-3T1, has frequently been reported at other Tethyan localities (Arenillas et al., 2000a, b, 2018; Keller, 2003; Coccioni et al., 2010; Punekar et al., 2014a,b), always above the onset of the biserial acme of PFAS-3 (here PFAS-3α). In addition, this acme has been reported in the Gulf of Mexico (Arz et al., 2001; Abramovich et al., 2011), in the North Pacific (Smit and Romein, 1985), in the Western North Atlantic (Mateo et al., 2016), and in the Parathetys (Punekar et al., 2016). Therefore, PFAS-3T1 probably characterizes a global response to environmental stress.

During PFAS3T-1, the low-oxygenated sub-thermocline dweller *Chiloguembelina* (Boersma and Premoli Silva, 1989; Olsson et al., 1999; Aze et al., 2011; Luciani et al., 2020) became more abundant than during PFAS-3α, suggesting the progressive reoccupation of the deeper-most niches initiated in PFAS-3α. *Chiloguembelina* stabilized in abundance through the section (Fig.

660 5 and Fig. 10B) suggesting that the oxygen minimum zone did not show major changes during
661 the studied interval. Nevertheless, near the end of PFAS3-T1 (around the onset of Dan-C2), the
662 *Braarudosphaera* bloom was followed by an acme of *Neobiscutum* species (Fig. 10B; Romein,
663 1977; Gardin and Monechi, 1998, Gardin, 2002; Lamolda et al., 2016; Thibault et al., 2018),
664 suggesting rapidly changing ecological conditions in the upper part of the water column during
665 the beginning of the Dan-C2 event.
666
667 Conversely to what may be expected, the minima of both Dan-C2 CIEs occurred during
668 PFAS-3O substages instead of during triserial blooms. This lack of coincidence between the
669 evidence for C-cycle perturbation and biotic stress was also noted in Italy (Coccioni et al., 2010)
670 and can also be observed in the data reported by Punekar et al. (2014a) from Israel, Egypt and the
671 USA. Since bulk $\delta^{18}O$ and $\delta^{13}C$ mostly reflect changes in the upper part of the water column it
672 can be assumed that transient surface water warming occurred during both CIEs. No evidence of
673 bottom water warming has been detected in the Dan-C2 interval, based on benthic foraminiferal
674 $\delta^{18}O$ (Fig. 9; see Barnet et al., 2019 and references therein). Instead, the warming indicated by
675 the bulk oxygen isotope data may have led to a rapid thermal stratification of the upper part of
676 the water column that caused a stronger thermal gradient between the near-surface waters and the
677 thermocline, creating more differentiated ecological niches. The increase of the deeper water
678 dwelling species (such as *Chiloguembelina*, *Eoglobigerina*, *Globanomalina* and *Parasubbotina*)
679 during both CIEs agrees with transient but enhanced ocean stratification (Fig. 5 and Figs. 10B,
680 10E). The overall planktic foraminiferal assemblage response during Dan-C2 interval is
681 represented by an alternation between the triserial blooms (PFAS-3T1, 2, 3) and increases in other
682 genera (PFAS3-O1, 2) which are progressively less abrupt through time (Fig. 8 and Fig. 10B).
683 These ecological alternations suggest rapidly changing conditions but also a slightly more
684 resilient and stable ocean, compared to the very earliest Danian. During the Dan-C2 event, $CaCO_3$
685 dissolution due to ocean acidification has been invoked (see Coccioni et al., 2010; Krahl et al.,
686 2020 and references therein) but, at Caravaca, the dissolution-sensitive parameters (fragmentation
687 index, $CaCO_3$ content and P/B ratio) do not show evidence of strong dissolution, although we

688 note that there are slight decreases in the $\%CaCO_3$ content and slight increases in the
689 fragmentation index within the Dan-C2 interval, roughly coincident with the two CIEs.
690
691 *5.5. End of PFAS-3: Shift to a more stable ocean*
692
693 The stabilization of the planktic foraminiferal assemblages at Caravaca seems to have been
694 completed in PFAS-3O3, although there are some differences in comparison to the previous
695 PFAS-3O substages. During PFAS-3O3, *Praemurica* significantly increases in abundance, and
696 the triserial *Chiloguembelitria* is replaced by the trochospiral guembelitriid *Globoconusa* (Fig. 5,
697 Fig. 10B and Table S2). The combined abundances of the *Chiloguembelitria* and *Globoconusa*
698 genera is lower than the abundance reached by *Chiloguembelitria* in any of the preceding acme
699 stages and substages, suggesting lower environmental stress conditions from PFAS-3O3 onwards.
700
701 During PFAS-3O3 newly incoming nannoplankton taxa become dominant, including the r-
702 selected opportunist *Futyana petalosa* and the first K-strategists *Cruciplacolithus* and
703 *Coccolithius* (Romein, 1977; Gardin, 2002; Thibault et al., 2018; Jiang et al., 2019).
704 *Cruciplacolithus* and *Coccolithius* are generally reported as oligotrophic taxa (Jiang et al., 2010,
705 2019), suggesting that the upper ocean waters at Caravaca became more oligotrophic during
706 PFAS-3O3. Oligotrophic conditions at Caravaca are also supported by the very low abundance
707 of *Chiloguembelitria* and by the rise of the *Praemurica* lineage, within which planktic
708 foraminifera species first acquire symbionts during the Paleocene (Norris, 1996; Birch et al.,
709 2012). In addition, carbonate content, magnetic susceptibility, fragmentation index, the P/B ratio
710 and isotopic proxies show only minor oscillations in PFAS-3O3, suggesting relatively stable
711 conditions (Fig. 8).

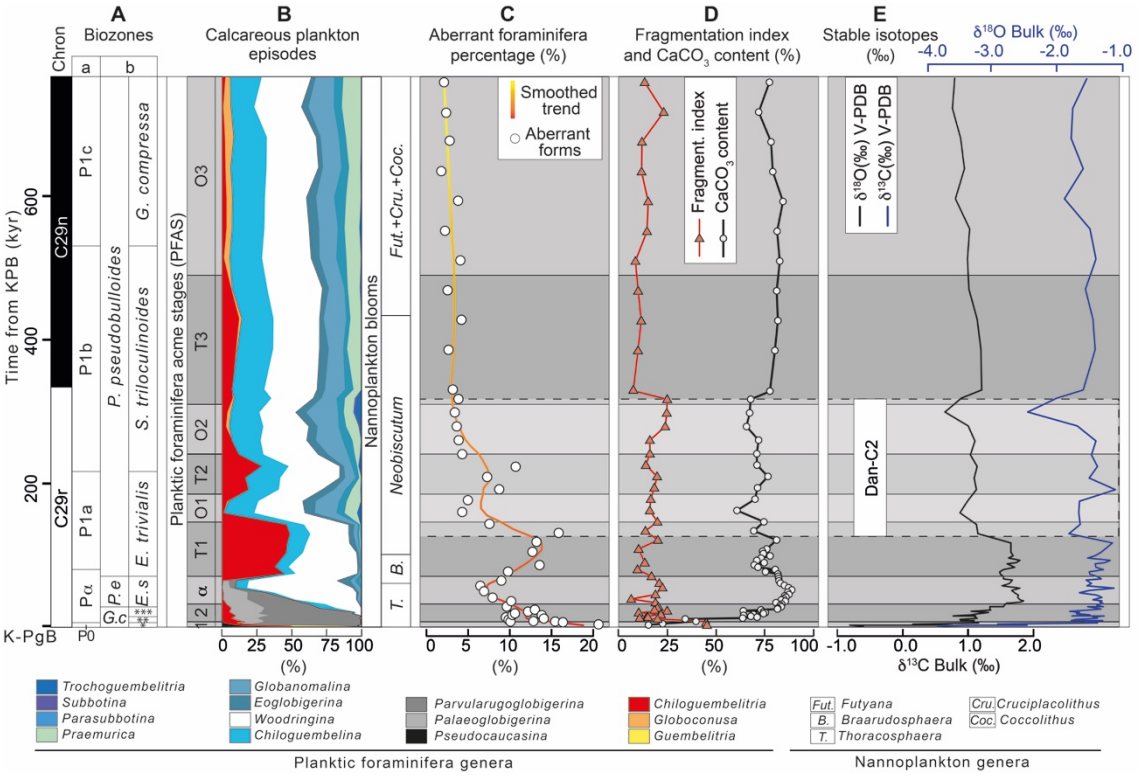

Fig. 10. Synthesis of the results obtained in this study: A) Planktic foraminiferal biozonations: a = Wade et al. (2011); b = Arenillas et al. (2004); B) Relative abundances of Danian planktic foraminiferal genera, and correlation of the planktic foraminiferal acme-stages (PFAS) and calcareous nannoplankton blooms (see references in the text); C) Relative abundance of planktic foraminiferal aberrant specimens; D) Main carbonate sensitivity parameters; E) Bulk carbonate stable isotopes.

6. What was the environmental impact of the Deccan Traps during the earliest Danian?

For several decades, identifying the role of the Deccan Traps (India) in environmental and climatic change across the K-PgB has been difficult, mainly due to the uncertainties associated with radioisotopic dating (e.g., Courtillot et al., 1986; Vandamme et al., 1991; Chenet et al., 2007). However, recent improvements in radiometric methods have led to refined estimates of the duration of Deccan volcanism, at less than 1 Myr (Schoene et al., 2019; Sprain et al., 2019), and allowed for a more robust correlation between volcanism and climate change (e.g., Barnet et al., 2018; Hernandez Nava et al., 2021). Whether the major eruptive episodes of the Deccan Traps occurred before or after the K-PgB remains a topic of intense debate, since the timing has

729 profound implications for the role of the Deccan Traps in the K-PgB mass extinction (Burgess,
730 2019; Hull et al., 2020; Keller et al., 2020). This controversy over the role of volcanism in the
731 extinction event is mostly related to uncertainty over the stratigraphic position of the K-PgB
732 within the Deccan Traps sequence.
733
734 Based on $^{40}Ar/^{39}Ar$ dating, Sprain et al. (2018) reported an age of 66.052 ± 0.008/0.043 for
735 the K-PgB, supporting the hypothesis that the most voluminous formations of the Deccan Traps,
736 which belong to the Wai subgroup (Poladpur, Ambenali and Mahabaleswar), are placed above
737 the K-PgB (Jay and Widdowson, 2008; Renne et al., 2015; Richards et al., 2015; Sprain et al.,
738 2019). According to the eruptive model of Sprain et al. (2019), the K-PgB is near the base of the
739 Poladpur Formation, and thus the most voluminous eruptive episodes of the Deccan Traps may
740 be early Danian in age. However, based on U-Pb dating, Clyde et al. (2016) reported an age of
741 66.021 ± 0.24/0.039 Ma for the K-PgB, supporting the emplacement of the Poladpur Formation
742 prior to the K-PgB (Schoene et al., 2015, 2019, 2021; Kasbohm et al., 2021; Fig. 11). According
743 to the eruptive model of Schoene et al. (2019), the emplacement of the Poladpur Formation,
744 (which achieved the highest eruption rate of Deccan volcanism) occurred in the latest
745 Maastrichtian, preceding the K-PgB by only some tens of thousands of years. Schoene et al.
746 (2021) recalculated the eruptive volumes of the model of Sprain et al. (2019) in terms of eruptive
747 rate (Fig. 11), which clearly distinguishes between the mega-pulse eruptive model of Schoene et
748 al. (2019) and the quasi-continuous eruptive model of Sprain et al. (2019).
749

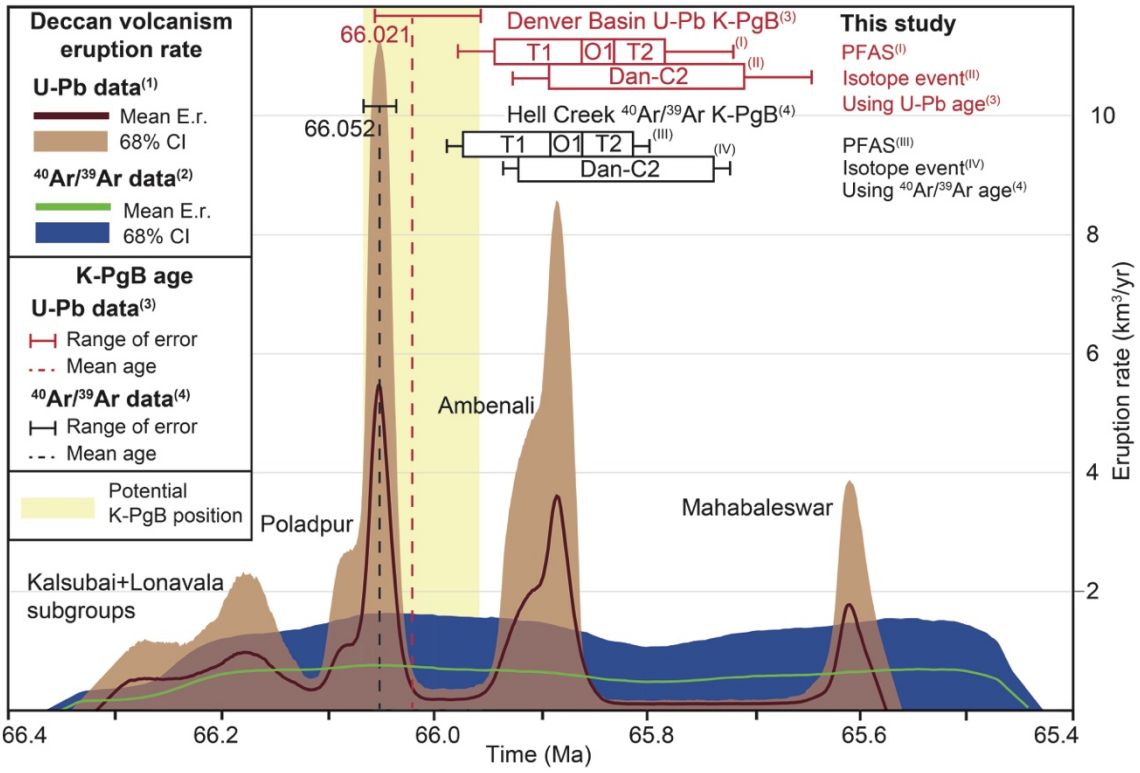

Fig. 11. Age models and eruption rates for the Deccan Traps based on Fig. 4 of Schoene et al. (2021), compared with the age of key early Danian paleontological and climatic events as determined in the Caravaca section. The yellow band shows the most probable stratigraphic range for the K-PgB position within the Deccan Traps, considering both the range of error on U-Pb and $^{40}Ar/^{39}Ar$ dates. Our preferred age model for Caravaca is anchored at the K-PgB using an $^{40}Ar/^{39}Ar$ age of 66.052 Ma, but we also show how the relationship between Deccan volcanism and the PFAS-3T1, 3O1 and 3T2 and Dan-C2 events could vary by changing the age of the K-PgB to that derived from U-Pb (66.021 Ma). Error margins for both radiometric techniques are also shown and incorporated into the age estimates of early Danian events. E.r. = eruption rate; CI =Confidence interval (1) = (Schoene et al., 2019); (2) = (Sprain et al., 2019); (3) = (Clyde et al., 2016); (4) = (Sprain et al., 2018).

The Rajahmundry Traps (RT, SE India) bear witness to the scale of early Danian Deccan volcanism, extending ~1000 km from the erupting center and forming the longest lava flows on Earth (Self et al., 2008; Keller et al., 2011, 2012). The exposed flows of the RT have been dated as early Danian in age (Keller et al., 2008; Fendley et al., 2020) and have been geochemically assigned to the Ambenali and Mahabaleshwar Formations in the Western Ghats (Baksi, 2001; Self et al., 2008). The age of the RT is also compatible with the recently published radiometric

768 ages of the Ambenali and Mahabaleshwar Formations (Schoene et al., 2019; Sprain et al., 2019).
769 However, the eruption and outgassing rates in each phase of Deccan volcanism are considered
770 potentially more important for climate change than the volume of basalt erupted (Self et al., 2006;
771 Gertsch et al., 2011; Hernandez Nava et al., 2021). Recent estimations of the amount and rates of
772 CO_2 release from Deccan volcanism predict only minor increases in atmospheric CO_2 compared
773 to the background Cretaceous–Paleogene atmospheric reservoir (Self et al., 2006; Schmidt et al.,
774 2016; Steinthorsdottir et al., 2016; Henehan et al., 2016; Fendley et al., 2020). Modelling of
775 different climate sensitivities and volcanic outgassing scenarios suggest that Deccan volcanism
776 alone was insufficient to have driven warming during the early Danian (Hull et al., 2020; Fendley
777 et al., 2020). Conversely, the influence of volcanic SO_2 and halogen emissions could have been
778 profound at times of flood basalt emplacement (Self et al., 2006). Although volcanic aerosols
779 have a short residence time in the troposphere of ~1 week, flood basalt activity could have
780 provided a semi-continuous SO_2 supply (Self et al., 2006), which may have resulted in cooling
781 and/or ocean acidification on geologic time scales (Gertsch et al., 2011; Courtillot and Fluteau,
782 2014).
783
784 Our data show no indications of ocean acidification or temperature changes in the first 50
785 kyr of the Danian, except within the K-PgB clay bed, and thus the effect of volcanic outgassing
786 directly following the Chicxulub impact (Renne et al., 2015; Sprain et al., 2019) may have been
787 obscured by the extinction of calcifying plankton (Henehan et al., 2019). Alternatively, our data
788 could indicate that there was no significant Deccan volcanic activity during the earliest Danian.
789 This would be in accordance with Schoene et al. (2019), who suggested that the Poladpur eruptive
790 pulse occurred in the latest Maastrichtian and was followed by a period of volcanic inactivity in
791 the Deccan for about 100 kyr, extending into the earliest Danian. The return to higher stressed
792 environmental conditions at Caravaca occurred ~70 kyr after the K-PgB, as evidenced by the
793 *Chiloguembelitria* bloom in PFAS-3T1, which is broadly coincident with the eruption of the
794 Ambenali Formation (Schoene et al., 2019; Sprain et al., 2019). Recent pH estimates, based on
795 boron isotopes, show initial surface water acidification after the K-PgB, followed by a rapid

796 rebound and overshoot in surface ocean pH within 40 kyr, before pH values returned to pre-K-
797 PgB background levels after ~120 kyr (Henehan et al., 2019). Previous ocean pH estimates
798 predicted a rise in pH due to the extinction of calcifying organisms and the consequent transient
799 reduction in the marine alkalinity sink (Caldeira et al., 1990; Henehan et al., 2016). The latter is
800 supported by observations of improved deep-sea carbonate preservation during the time of the pH
801 overshoot (e.g. Minoletti et al., 2005; Alegret and Thomas, 2013; Tobin et al., 2017) and by our
802 own data (see section 5.1 and 5.2).
803
804 At Caravaca, the aberrant index follows a declining trend during the first ~70 kyr of the
805 Danian, from PFAS-1 to PFAS-3α, suggesting a reduction in the impact of the different
806 environmental stressors with a rapid recovery of productivity. Conversely, during the following
807 ~80 kyr (in PFAS-3T1), the opportunistic *Chiloguembelitria* bloomed at a global scale, and the
808 aberrant index increased again (see section 5.4), suggesting a new episode of environmental
809 stress. Commonly, guembelitriid blooms are reported from shallow marine areas, often near
810 volcanic provinces with a high nutrient flux (Pardo and Keller, 2008). However, these
811 opportunistic taxa radiated and proliferated in the pelagic realm after the K-PgB (Olsson et al.,
812 1999; Arenillas et al., 2000a,b; Keller, 2003), suggesting that, during the early Danian, their
813 ecological preferences of high nutrient availability were met in the open ocean. Although the
814 uncertainties in the temporal correlation between Deccan Traps volcanic phases, the K-PgB, and
815 climatic and paleobiological events are still significant, our data suggest that the
816 *Chiloguembelitria* bloom (PFAS-3T1) is coeval with the emplacement of the Ambenali
817 Formation (Fig. 11).
818
819 The emplacement of the Ambenali formation and the apparent co-occurrence with the Dan-
820 C2 event in the upper part of C29r (Fig. 10A and 10D), has led some authors to link these two
821 events mechanistically (Coccioni et al., 2010; Krahl et al., 2020; Punekar et al., 2014a). However,
822 the Dan-C2 event was not associated with bottom water warming (Quillévéré et al., 2008;
823 Coccioni et al., 2010; Barnet et al., 2019; Krahl et al., 2020) which raises questions as to whether

824 this event can be considered a 'true' hyperthermal event or not (see discussion in Barnet et al.,
825 2019). Ocean acidification has also been invoked during Dan-C2 (Coccioni et al., 2010; Krahl et
826 al., 2020) but no convincing evidence has been identified during the Dan-C2 interval at Caravaca
827 nor in other sections to support this (see Barnet et al., 2019). The exact mechanisms that drove
828 the Dan-C2 event are poorly resolved, and several hypotheses have been put forward: pulses of
829 massive Deccan volcanic eruptions (Krahl et al., 2020); a combination of Deccan volcanism with
830 an orbital configuration which perturbed the carbon cycle (e.g. Coccioni et al., 2010; Barnet et
831 al., 2019; Sinnesael et al., 2019); and/or passive degassing of CO_2 due to the interaction of
832 intrusive magma bodies with the crust (see Sprain et al., 2019; Fendley et al., 2020). The quasi-
833 continuous eruptive model suggests that the Ambenali Formation represents a relatively long
834 volcanic episode (Renne et al., 2015; Sprain et al., 2019). Although this scenario does not provide
835 a relatively rapid trigger mechanism for environmental change, it still permits a hypothesis that
836 the Deccan volcanism could add to emissions of CO_2 by passive degassing over longer timescales,
837 contributing, albeit perhaps in a minor way, to early Danian climate change and the Dan-C2 event.
838 Conversely, the hypothesis of a shorter (<100 kyr), more intense, volcanic pulse (Schoene et al.,
839 2019) is not supported by geochemical evidence from marine records (Hull et al., 2020), and
840 would imply a minimal impact of volcanic activity on climate. Regardless of the eruptive model
841 favoured, and considering the estimated duration for the Ambelani eruptive episode, volcanic
842 outgassing from the Deccan Traps by itself was probably insufficient to drive significant warming
843 during the early Danian (Fendley et al., 2020; Hull et al., 2020), although it may have exacerbated
844 environmental stress. Our age model allows us to suggest that the Ambenali phase coincided with
845 the first Dan-C2 CIE, but not with the second CIE (Fig. 11). If Deccan volcanism was not the
846 cause of the second CIE, then it seems that other factors, such as orbital forcing, are required to
847 fully explain the Dan-C2 event.
848
849 Since the proposed warming for the Dan-C2 event is only observed in bulk and planktic
850 foraminiferal isotopic records (Fig. 9), the increase in temperature probably only affected surface
851 ocean waters. A transient but enhanced thermal stratification of the upper part of the water column

may have resulted in more differentiated ecological niches. This is supported by our data at Caravaca, which show rapid turnovers of planktic foraminiferal assemblages in PFAS-3O1 and O2 coinciding approximately with both Dan-C2 CIEs. Remarkably, continental records of the first ~700 kyr of the Danian have documented increases in ecologic diversification of plants and mammals (suggested by increased species richness and taxonomic composition), coinciding with the warmer intervals of the early Danian (Lyson et al., 2019; Chiarenza et al., 2020). Therefore, if the Dan-C2 event influenced both marine and terrestrial ecosystems (driven by Deccan volcanism, orbital forcing, or a combination of those and additional mechanisms), it did not cause harmful environmental effects, but instead may have temporarily boosted the recovery of ecosystems.

6. Conclusions

High-resolution planktic foraminiferal, geochemical and paleomagnetic analyses of the first ~750 kyr of the Danian at Caravaca (Spain, western Tethys) were carried out. Planktic foraminiferal assemblages after the Cretaceous-Paleogene boundary (K-PgB) are characterized by a rapid succession of planktic foraminiferal acme-stages (PFAS). The first acme is of the triserial *Guembelitria* (PFAS-1), the second of the tiny trochospiral *Parvularugoglobigerina-Palaeoglobigerina* (PFAS-2), and the third of the biserial *Woodringina-Chiloguembelina* (PFAS-3). Within PFAS-3, seven shorter substages are distinguished: PFAS-3α during the maximal bloom of biserials, PFAS-3T1, T2 and T3 for blooms of the triserial *Chiloguembelitria*, and PFAS-3O1, O2, O3 for increases in abundance of the trochospiral genera *Eoglobigerina*, *Praemurica*, *Globanomalina* and *Parasubbotina*. Triserial blooms and a high abundance of aberrant forms are striking evidence of enhanced environmental stress, occurring especially within PFAS-1 and PFAS-3T substages, during the first 230 kyr of the Danian.

On the basis of $\delta^{18}O$ and $\delta^{13}C$, $CaCO_3$ content and magnetic susceptibility, the Dan-C2 event has been identified for the first time at the Caravaca section. The two carbon isotopic excursions

(CIEs) that characterize the Dan-C2 event have been linked to surface water warming that caused enhanced thermal stratification. During both CIEs, the PFAS-3T assemblages were rapidly replaced by the PFAS-3O assemblages containing less opportunistic taxa, probably because the water depth habitats became more differentiated. High carbonate dissolution is restricted to the K-PgB clay bed, while the Dan-C2 event and the rest of the section show no evidence of significant carbonate dissolution episodes. Although there are still uncertainties in radiometric dating, our data suggest that the first and largest *Chiloguembelitria* bloom (PFAS-3T1) coincided with the emplacement of the Ambenali Formation of the Deccan Traps. Conversely, the Dan-C2 event was decoupled from both the Ambenali eruptive pulse and the *Chiloguembelitria* bloom, starting long after these events had occurred. This suggests that volcanic outgassing of CO_2 was insufficient to drive warming, which only occurred only when the effects of volcanic CO_2 were combined with other factors such as a specific orbital configuration. More high-resolution multidisciplinary studies are needed to fully assess the relationship between Deccan Traps volcanism on early Danian climate, and its potential contribution in reshaping life on Earth after the end-Cretaceous mass extinction.

Acknowledgements

This work was supported by MCIU/AEI/FEDER, UE (grant number PGC2018-093890-B-I00), and by the Aragonian Government/FEDER, UE (grant number DGA groups E33_17R and E33_20R). Vicente Gilabert acknowledges support from the Spanish Ministerio de Economía, Industria y Competitividad (FPI grant number BES-2016-077800). The authors would like to acknowledge the use of the Servicio General de Apoyo a la Investigación-SAI, Universidad de Zaragoza. This research is part of the PhD thesis of the first author.

References

Abramovich, S., Keller, G., Berner, Z., Cymbalista, M., Rak, C., 2011. Maastrichtian Planktic Foraminiferal Biostratigraphy and Paleoenvironment of Brazos River, Falls County, Texas, U.S.A., in: Keller, G., Adatte, T. (Eds.), The End-Cretaceous Mass Extinction and the Chicxulub Impact in Texas. SEPM (Society for Sedimentary Geology), Tulsa, pp. 123-156. https://doi.org/10.2110/sepmsp.100.123.

Alegret, L., Thomas, E., 2013. Benthic foraminifera across the Cretaceous/Paleogene boundary in the Southern Ocean (ODP Site 690): Diversity, food and carbonate saturation. Mar. Micropaleontol. 105, 40-51. https://doi.org/10.1016/j.marmicro.2013.10.003.

Alegret, L., Molina, E., Thomas, E., 2003. Benthic foraminiferal turnover across the Cretaceous/Paleogene boundary at Agost (southeastern Spain): Paleoenvironmental inferences. Mar. Micropaleontol. 48, 251-279. https://doi.org/10.1016/S0377-8398(03)00022-7.

Alegret, L., Thomas, E., Lohmann, K.C., 2012. End-Cretaceous marine mass extinction not caused by productivity collapse. Proc. Natl. Acad. Sci. USA 109, 728-732. https://doi.org/10.1073/pnas.1110601109.

Alvarez, L.W., Alvarez, W., Asaro, F., Michel, H. V., 1980. Extraterrestrial cause for the Cretaceous-Tertiary extinction. Science 208, 1095-1108. https://doi.org/10.1126/science.208.4448.1095.

Andeweg, B., 2002. Cenozoic tectonic evolution of the Iberian Peninsula: effects and causes of changing stress fields. PhD thesis, Vrije Universiteit Amsterdam, Amsterdam, 192 pp.

Arenillas, I., Arz, J.A., 2017. Benthic origin and earliest evolution of the first planktonic foraminifera after the Cretaceous/Palaeogene boundary mass extinction. Hist. Biol. 29, 25-42. https://doi.org/10.1080/08912963.2015.1119133.

929 Arenillas, I., Arz, J.A., Molina, E., 1998. El límite Cretácico/Terciario de Zumaya, Osinaga y
930 Músquiz (Pirineos): control bioestratigráfico y cuantitativo de hiatos con foraminíferos
931 planctónicos. Rev. Soc. Geol. Esp. 11(1-2), 127-138.

932 Arenillas, I., Arz, J.A., Molina, E., Dupuis, C., 2000a. The Cretaceous/Paleogene (K/P)
933 boundary at Aïn Settara, Tunisia: Sudden catastrophic mass extinction in planktic
934 foraminifera. J. Foraminifer. Res. 30, 202-218. https://doi.org/10.2113/0300202.

935 Arenillas, I., Arz, J.A., Molina, E., Dupuis, C., 2000b. An independent test of planktic
936 foraminiferal turnover across the Cretaceous/Paleogene (K/P) boundary at El Kef, Tunisia:
937 Catastrophic mass extinction and possible survivorship. Micropaleontology 46, 31-49.

938 Arenillas, I., Arz, J.A., Molina, E., 2004. A new high-resolution planktic foraminiferal zonation
939 and subzonation for the lower Danian. Lethaia 37, 79-95.
940 https://doi.org/10.1080/00241160310005097.

941 Arenillas, I., Arz, J.A., Grajales-Nishimura, J.M., Murillo-Muñetón, G., Alvarez, W., Camargo-
942 Zanoguera, A., Molina, E., Rosales-Domínguez, C., 2006. Chicxulub impact event is
943 Cretaceous/Paleogene boundary in age: New micropaleontological evidence. Earth Planet.
944 Sci. Lett. 249, 241-257. https://doi.org/10.1016/j.epsl.2006.07.020.

945 Arenillas, I., Arz, J.A., Grajales-Nishimura, J.M., Meléndez, A., Rojas-Consuegra, R., 2016.
946 The Chicxulub impact is synchronous with the planktonic foraminifera mass extinction at
947 the Cretaceous/Paleogene boundary: New evidence from the Moncada section, Cuba.
948 Geol. Acta 14, 35-51. https://doi.org/10.1344/GeologicaActa2016.14.1.4.

949 Arenillas, I., Arz, J.A., Gilabert, V., 2018. Blooms of aberrant planktic foraminifera across the
950 K/Pg boundary in the Western Tethys: Causes and evolutionary implications.
951 Paleobiology 44, 460-489. https://doi.org/10.1017/pab.2018.16.

952 Arz, J.A., Arenillas, I., Molina, E., Sepúlveda, R., 2000. La estabilidad evolutiva de los
953 foraminíferos planctónicos en el Maastrichtiense superior y su extinción en el límite
954 Cretácico/Terciario de Caravaca, España. Rev. geol. Chile 27, 27-47.
955 http://dx.doi.org/10.4067/S0716-02082000000100003.

956 Arz, J.A., Alegret, L., Arenillas, I., Liesa, C., Molina, E., Soria, A.R., 2001. Extinción de
957 foraminíferos del límite Cretácico/Terciario en Coxquihui (México) y su relación con las
958 evidencias de impacto. Rev. Esp. Micropaleontol. 33(2), 221-236.

959 Ashckenazi-Polivoda, S., Rak, C., Almogi-Labin, A., Zsolt, B., Ovadia, O., Abramovich, S.,
960 2014. Paleoecology of the K-Pg mass extinction survivor *Guembelitria* (Cushman):
961 isotopic evidence from pristine foraminifera from Brazos River, Texas (Maastrichtian).
962 Paleobiology 40, 24-33. https://doi.org/10.1666/13317.

963 Aze, T., Ezard, T.H.G., Purvis, A., Coxall, H.K., Stewart, D.R.M., Wade, B.S., Pearson, P.N.,
964 2011. A phylogeny of Cenozoic macroperforate planktonic foraminifera from fossil data.
965 Biol. Rev. 86, 900-927. https://doi.org/10.1111/j.1469-185X.2011.00178.x.

966 Ballent, S.C., Carignano, A.P., 2008. Morphological abnormalities in Late Cretaceous and early
967 Paleocene foraminifer tests (northern Patagonia, Argentina). Mar. Micropaleontol. 67,
968 288-296. https://doi.org/10.1016/j.marmicro.2008.02.003.

969 Baksi, A.K., 2001. The Rajahmundry Traps, Andhra Pradesh: Evaluation of their petrogenesis
970 relative to the Deccan Traps. Proc. Indian Acad. Sci. Earth Planet. Sci. 110, 397-407.
971 https://doi.org/10.1007/BF02702903.

972 Barnet, J.S.K., Littler, K., Kroon, D., Leng, M.J., Westerhold, T., Röhl, U., Zachos, J.C., 2018.
973 A new high-resolution chronology for the late Maastrichtian warming event: Establishing
974 robust temporal links with the onset of Deccan volcanism. Geology 46, 147-150.
975 https://doi.org/10.1130/G39771.1.

976 Barnet, J.S.K., Littler, K., Westerhold, T., Kroon, D., Leng, M.J., Bailey, I., Röhl, U., Zachos,
977 J.C., 2019. A High-Fidelity Benthic Stable Isotope Record of Late Cretaceous-Early
978 Eocene Climate Change and Carbon-Cycling. Paleoceanogr. Paleoclimatology 34, 672-
979 691. https://doi.org/10.1029/2019PA003556.

980 Beals, E.W., 1984. Bray-Curtis ordination: An effective strategy for analysis of multivariate
981 ecological data. Adv. Ecol. Res. 14, 1-55. https://doi.org/10.1016/S0065-2504(08)60168-
982 3.

983 Berger, W.H., Bonneau, M., Parker, F.L., Plateau, L., 1982. Foraminifera on the deep-sea floor:
984 lysocline and dissolution rate. Oceanol. Acta 5, 249-258.

985 Berggren, W.A., Pearson, P.N., 2005. A revised tropical to subtropical Paleogene planktonic
986 foraminiferal zonation. J. Foraminifer. Res. 35, 279-298. https://doi.org/10.2113/35.4.279.

987 Birch, H.S., Coxall, H.K., Pearson, P.N., 2012. Evolutionary ecology of Early Paleocene
988 planktonic foraminifera: size, depth habitat and symbiosis. Paleobiology 38, 374-390.
989 https://doi.org/10.1666/11027.1.

990 Birch, H.S., Coxall, H.K., Pearson, P.N., Kroon, D., Schmidt, D.N., 2016. Partial collapse of the
991 marine carbon pump after the Cretaceous-Paleogene boundary. Geology 44, 287-290.
992 https://doi.org/10.1130/G37581.1.

993 Boersma, A., Premoli Silva, I., 1989. Atlantic Paleogene biserial heterohelicid foraminifera and
994 oxygen minima. Paleoceanography 4, 271-286.

995 Bown, P., 2005. Selective calcareous nannoplankton survivorship at the Cretaceous-Tertiary
996 boundary. Geology 33, 653-656. https://doi.org/10.1130/G21566.1.

997 Burgess, S., 2019. Deciphering mass extinction triggers. Science 363, 815-816.
998 https://doi.org/10.1126/science.aaw0473.

999 Bralower, T.J., Cosmidis, J., Heaney, P.J., Kump, L.R., Morgan, J. V., Harper, D.T., Lyons,
1000 S.L., Freeman, K.H., Grice, K., Wendler, J.E., Zachos, J.C., Artemieva, N., Chen, S.A.,
1001 Gulick, S.P.S., House, C.H., Jones, H.L., Lowery, C.M., Nims, C., Schaefer, B., Thomas,
1002 E., Vajda, V., 2020. Origin of a global carbonate layer deposited in the aftermath of the
1003 Cretaceous-Paleogene boundary impact. Earth Planet. Sci. Lett. 548, 116476.
1004 https://doi.org/10.1016/j.epsl.2020.116476.

1005 Bukry, D., 1974. Coccoliths as paleosalinity indicators - evidence from Black Sea, in: Degens,
1006 E.T., Ross. D.A. (Eds.), The Black Sea–Geology, Chemistry, and Biology. AAPG Memoir
1007 20, Tulsa, pp. 353-363.

1008 Caldeira, K., Rampino, M.R., Volk, T., Zachos, J.C., 1990. Biogeochemical modeling at mass
1009 extinction boundaries: Atmospheric carbon dioxide and ocean alkalinity at the K/T
1010 boundary, in: Kauffman E.G., Walliser O.H. (Eds), Extinction Events in Earth History.
1011 Lecture Notes in Earth Sciences, 30, Springer, Berlin, Heidelberg, pp. 333-345.
1012 https://doi.org/10.1007/bfb0011156.

1013 Canudo, J.I., Keller, G., Molina, E., 1991. Cretaceous/Tertiary boundary extinction pattern and
1014 faunal turnover at Agost and Caravaca, S.E. Spain. Mar. Micropaleontol. 17, 319-341.
1015 https://doi.org/10.1016/0377-8398(91)90019-3.

1016 Chenet, A.L., Quidelleur, X., Fluteau, F., Courtillot, V., Bajpai, S., 2007. ^{40}K-^{40}Ar dating of the
1017 Main Deccan large igneous province: Further evidence of KTB age and short duration.
1018 Earth Planet. Sci. Lett. 263, 1-15. https://doi.org/10.1016/j.epsl.2007.07.011.

1019 Chiarenza, A.A., Farnsworth, A., Mannion, P.D., Lunt, D.J., Valdes, P.J., Morgan, J. V.,
1020 Allison, P.A., 2020. Asteroid impact, not volcanism, caused the end-Cretaceous dinosaur
1021 extinction. Proc. Natl. Acad. Sci. USA 117, 17084-17093.
1022 https://doi.org/10.1073/pnas.2006087117.

1023 Clyde, W.C., Ramezani, J., Johnson, K.R., Bowring, S.A., Jones, M.M., 2016. Direct high-
1024 precision U-Pb geochronology of the end-Cretaceous extinction and calibration of
1025 Paleocene astronomical timescales. Earth Planet. Sci. Lett. 452, 272-280.
1026 https://doi.org/10.1016/j.epsl.2016.07.041.

1027 Coccioni, R., Galeotti, S., 1994. K-T boundary extinction: Geologically instantaneous or
1028 gradual event? Evidence from deep-sea benthic foraminifera. Geology 22, 779-782.
1029 https://doi.org/10.1130/0091-7613(1994)022<0779:KTBEGI>2.3.CO;2.

1030 Coccioni, R., Luciani, V., 2006. *Guembelitria irregularis* bloom at the K-T boundary:
1031 Morphological abnormalities induced by impact-related extreme environmental stress?, in:
1032 Cockell, C., Gilmour, I., Koeberl, C. (Eds.), Biological Processes Associated with Impact
1033 Events. Springer-Verlag, Berlin, pp. 179-196. https://doi.org/10.1007/3-540-25736-5_8

1034 Coccioni, R., Frontalini, F., Bancalà, G., Fornaciari, E., Jovane, L., Sprovieri, M., 2010. The
1035 Dan-C2 hyperthermal event at Gubbio (Italy): Global implications, environmental effects,
1036 and cause(s). Earth Planet. Sci. Lett. 297, 298-305.
1037 https://doi.org/10.1016/j.epsl.2010.06.031.

1038 Courtillot, V., Besse, J., Vandamme, D., Montigny, R., Jaeger, J.-J., Cappetta, H., 1986. Deccan
1039 flood basalts at the Cretaceous/Tertiary boundary? Earth Planet. Sci. Lett. 80, 361–374.

1040 Courtillot, V., Fluteau, F., 2014. A review of the embedded time scales of flood basalt
1041 volcanism with special emphasis on dramatically short magmatic pulses, in: Keller, G.,
1042 Kerr, A.C. (Eds.), Volcanism, Impacts, and Mass Extinctions: Causes and Effects. Geol.
1043 Soc. Am. Spec. Pap. 505, p. 301-317. https://doi.org/10.1130/2014.2505(15).

1044 Coxall, H.K., D'Hondt, S., Zachos, J.C., 2006. Pelagic evolution and environmental recovery
1045 after the Cretaceous-Paleogene mass extinction. Geology 34, 297-300.
1046 https://doi.org/10.1130/G21702.1.

Cunha, A.S., Shimabukuro, S., 1997. *Braarudosphaera* blooms and anomalous enrichments of *Nannoconus*: evidence from the Turonian South Atlantic, Santos Basin, Brazil. J. Nannoplankt. Res. 19, 51-55.

D'Hondt, S., Donaghay, P., Zachos, J.C., Luttenberg, D., Lindinger, M., 1998. Organic carbon fluxes and ecological recovery from the Cretaceous-Tertiary mass extinction. Science 282, 276-279. https://doi.org/10.1126/science.282.5387.276.

Ellwood, B.B., Tomkin, J.H., Ratcliffe, K.T., Wright, M., Kafafy, A.M., 2008. High-resolution magnetic susceptibility and geochemistry for the Cenomanian/Turonian boundary GSSP with correlation to time equivalent core. Palaeogeogr. Palaeoclimatol. Palaeoecol. 261, 105-126. https://doi.org/10.1016/j.palaeo.2008.01.005.

Fendley, I.M., Sprain, C.J., Renne, P.R., Arenillas, I., Arz, J.A., Gilabert, V., Self, S., Vanderkluysen, L., Pande, K., Smit, J., Mittal, T., 2020. No Cretaceous-Paleogene boundary in exposed Rajahmundry Traps: A refined chronology of the longest Deccan lava flows from $^{40}Ar/^{39}Ar$ dates, magnetostratigraphy, and biostratigraphy. Geochemistry, Geophys. Geosystems 21, 1-20. https://doi.org/10.1029/2020gc009149.

Font, E., Adatte, T., Sial, A.N., de Lacerda, L.D., Keller, G., Punekar, J., 2016. Mercury anomaly, Deccan volcanism, and the end-Cretaceous mass extinction. Geology 44, 171-174. https://doi.org/10.1130/G37451.1.

Font, E., Adatte, T., Andrade, M., Keller, G., Mbabi Bitchong, A., Carvallo, C., Ferreira, J., Diogo, Z., Mirão, J., 2018. Deccan volcanism induced high-stress environment during the Cretaceous–Paleogene transition at Zumaia, Spain: Evidence from magnetic, mineralogical and biostratigraphic records. Earth Planet. Sci. Lett. 484, 53-66. https://doi.org/10.1016/j.epsl.2017.11.055.

1071 Fornaciari, E., Giusberti, L., Luciani, V., Tateo, F., Agnini, C., Backman, J., Oddone, M., Rio,
1072 D., 2007. An expanded Cretaceous-Tertiary transition in a pelagic setting of the Southern
1073 Alps (central-western Tethys). Palaeogeogr. Palaeoclimatol. Palaeoecol. 255, 98-131.
1074 https://doi.org/10.1016/j.palaeo.2007.02.044.

1075 Gallala, N., Zaghbib-Turki, D., Arenillas, I., Arz, J.A., Molina, E., 2009. Catastrophic mass
1076 extinction and assemblage evolution in planktic foraminifera across the
1077 Cretaceous/Paleogene (K/Pg) boundary at Bidart (SW France). Mar. Micropaleontol. 72,
1078 196-209. https://doi.org/10.1016/j.marmicro.2009.05.001.

1079 Gardin, S., 2002. Late Maastrichtian to early Danian calcareous nannofossils at Elles
1080 (Northwest Tunisia). A tale of one million years across the K-T boundary. Palaeogeogr.
1081 Palaeoclimatol. Palaeoecol. 178, 211-231. https://doi.org/10.1016/S0031-0182(01)00397-
1082 2.

1083 Gardin, S., Monechi, S., 1998. Palaeoecological change in middle to low latitude calcareous
1084 nannoplankton at the Cretaceous/Tertiary boundary. Bull. Soc. géol. Fr. 169, 709-723.

1085 Gerstel, J., Thunell, R.C., Zachos, J.C., Arthur, M.A., 1986. The Cretaceous/Tertiary boundary
1086 event in the North Pacific: Planktonic foraminiferal results from Deep Sea Drilling Project
1087 Site 577, Shatsky Rise. Paleoceanography 1, 97-117.
1088 https://doi.org/10.1029/PA001i002p00097.

1089 Gertsch, B., Keller, G., Adatte, T., Garg, R., Prasad, V., Berner, Z., Fleitmann, D., 2011.
1090 Environmental effects of Deccan volcanism across the Cretaceous-Tertiary transition in
1091 Meghalaya, India. Earth Planet. Sci. Lett. 310, 272-285.
1092 https://doi.org/10.1016/j.epsl.2011.08.015.

1093 Gibbs, S.J., Bown, P.R., Ward, B.A., Alvarez, S.A., Kim, H., Archontikis, O.A., Sauterey, B.,
1094 Poulton, A.J., Wilson, J., Ridgwell, A., 2020. Algal plankton turn to hunting to survive

and recover from end-Cretaceous impact darkness. Sci. Adv. 6, eabc9123. https://doi.org/10.1126/sciadv.abc9123.

Gilabert, V., Arz, J.A., Arenillas, I., Robinson, S.A., 2021. Influence of the Latest Maastrichtian Warming Event on planktic foraminiferal assemblages and ocean carbonate saturation at Caravaca, Spain. Cretac. Res. 125, 104844. https://doi.org/10.1016/j.cretres.2021.104844

Groot, J.J., de Jonge, R.B.G., Langereis, C.G., ten Kate, W.G.H.Z., Smit, J., 1989. Magnetostratigraphy of the Cretaceous-Tertiary boundary at Agost (Spain). Earth Planet. Sci. Lett. 94, 385-397. https://doi.org/10.1016/0012-821X(89)90155-6.

Gulick, S.P.S., Bralower, T.J., Ormö, J., Hall, B., Grice, K., Schaefer, B., Lyons, S., Freeman, K.H., Morgan, J. V., Artemieva, N., Kaskes, P., De Graaff, S.J., Whalen, M.T., Collins, G.S., Tikoo, S.M., Verhagen, C., Christeson, G.L., Claeys, P., Coolen, M.J.L., Goderis, S., Goto, K., Grieve, R.A.F., McCall, N., Osinski, G.R., Rae, A.S.P., Riller, U., Smit, J., Vajda, V., Wittmann, A., 2019. The first day of the Cenozoic. Proc. Natl. Acad. Sci. USA 116, 19342-19351. https://doi.org/10.1073/pnas.1909479116.

Hammer, Ø., Harper, D.A.T., Ryan, P.D., 2001. PAST: Paleontological statistics software package for education and data analysis. Paleontol. Electron. 4 (1), 9.

Henehan, M.J., Hull, P.M., Penman, D.E., Rae, J.W.B., Schmidt, D.N., 2016. Biogeochemical significance of pelagic ecosystem function: An end-Cretaceous case study. Philos. Trans. R. Soc. B Biol. Sci. 371. https://doi.org/10.1098/rstb.2015.0510.

Henehan, M.J., Ridgwell, A., Thomas, E., Zhang, S., Alegret, L., Schmidt, D.N., Rae, J.W.B., Witts, J.D., Landman, N.H., Greene, S.E., Huber, B.T., Super, J.R., Planavsky, N.J., Hull, P.M., 2019. Rapid ocean acidification and protracted Earth system recovery followed the end-Cretaceous Chicxulub impact. Proc. Natl. Acad. Sci. USA 116, 22500-22504. https://doi.org/10.1073/pnas.1905989116.

Hernandez Nava, A., Black, B.A., Gibson, S.A., Bodnar, R.J., Renne, P.R., Vanderkluysen, L., 2021. Reconciling early Deccan Traps CO_2 outgassing and pre-KPB global climate. Proc. Natl. Acad. Sci. USA 118, e2007797118. https://doi.org/10.1073/pnas.2007797118.

Hildebrand, A.R., Penfield, G.T., Kring, D.A., Pilkington, M., Antonio, C.Z., Boynton, W. V., 1991. Chicxulub crater: A possible Cretaceous/Tertiary boundary impact crater on the Yucatan peninsula, Mexico. Geology 19, 867-871. https://doi.org/10.1130/0091-7613(1991)019<0867:CCAPCT>2.3.CO;2.

Huber, B.T., MacLeod, K.G., Norris, R.D., 2002. Abrupt extinction and subsequent reworking of Cretaceous planktonic foraminifera across the Cretaceous-Tertiary boundary: Evidence from the subtropical North Atlantic. Geol. Soc. Am. Spec. Pap. 356, 277-289. https://doi.org/10.1130/0-8137-2356-6.277.

Hull, P.M., Bornemann, A., Penman, D.E., Henehan, M.J., Norris, R.D., Wilson, P.A., Blum, P., Alegret, L., Batenburg, S.J., Bown, P.R., Bralower, T.J., Cournede, C., Deutsch, A., Donner, B., Friedrich, O., Jehle, S., Kim, H., Kroon, D., Lippert, P.C., Loroch, D., Moebius, I., Moriya, K., Peppe, D.J., Ravizza, G.E., Röhl, U., Schueth, J.D., Sepúlveda, J., Sexton, P.F., Sibert, E.C., Śliwińska, K.K., Summons, R.E., Thomas, E., Westerhold, T., Whiteside, J.H., Yamaguchi, T., Zachos, J.C., 2020. On impact and volcanism across the Cretaceous-Paleogene boundary. Science 367, 266-272. https://doi.org/10.1126/science.aay5055.

Jay, A.E., Widdowson, M., 2008. Stratigraphy, structure and volcanology of the SE Deccan continental flood basalt province: Implications for eruptive extent and volumes. J. Geol. Soc. London. 165, 177-188. https://doi.org/10.1144/0016-76492006-062.

Jiang, S., Bralower, T.J., Patzkowsky, M.E., Kump, L.R., Schueth, J.D., 2010. Geographic controls on nannoplankton extinction across the Cretaceous/Palaeogene boundary. Nat. Geosci. 3, 280-285. https://doi.org/10.1038/ngeo775.

1144 Jiang, S., Chen, X., Bernaola, G., 2019. Environmental controls on calcareous nannoplankton
1145 response to the Cretaceous/Paleogene mass extinction in the Tethys realm. Palaeogeogr.
1146 Palaeoclimatol. Palaeoecol. 515, 134-142. https://doi.org/10.1016/j.palaeo.2017.12.044.

1147 Jones, H.L., Lowery, C.M., Bralower, T.J., 2019. Delayed calcareous nannoplankton boom-bust
1148 successions in the earliest Paleocene Chicxulub (Mexico) impact crater. Geology 47, 753-
1149 756. https://doi.org/10.1130/G46143.1.

1150 Kaiho, K., Lamolda, M.A., 1999. Catastrophic extinction of planktonic foraminifera at the
1151 Cretaceous-Tertiary boundary evidenced by stable isotopes and foraminiferal abundance at
1152 Caravaca, Spain. Geology 27, 355-358. https://doi.org/10.1130/0091-
1153 7613(1999)027<0355:CEOPFA>2.3.CO;2.

1154 Kaiho, K., Kajiwara, Y., Tazaki, K., Ueshima, M., Takeda, N., Kawahata, H., Arinobu, T.,
1155 Ishiwatari, R., Hirai, A., Lamolda, M.A., 1999. Oceanic primary productivity and
1156 dissolved oxygen levels at the Cretaceous/Tertiary boundary: Their decrease, subsequent
1157 warming, and recovery. Paleoceanography 14, 511-524.
1158 https://doi.org/10.1029/1999PA900022.

1159 Kasbohm, J., Schoene, B., Burgess, S., 2021. Radiometric constraints on the timing, tempo, and
1160 effects of large igneous province emplacement, in: Ernst, R.E., Dickson, J., Bekker, A.
1161 (Eds.), Large Igneous Provinces: A Driver of Global Environmental and Biotic Changes.
1162 American Geophysical Union. Carbon in Earth's Interior published by John Wiley & Sons,
1163 Inc., pp. 27-82. https://doi.org/https://doi.org/10.1002/9781119507444.ch2.

1164 Kawaragi, K., Sekine, Y., Kadono, T., Sugita, S., Ohno, S., Ishibashi, K., Kurosawa, K., Matsui,
1165 T., Ikeda, S., 2009. Direct measurements of chemical composition of shock-induced gases
1166 from calcite: an intense global warming after the Chicxulub impact due to the indirect
1167 greenhouse effect of carbon monoxide. Earth Planet. Sci. Lett. 282, 56-64.
1168 https://doi.org/10.1016/j.epsl.2009.02.037.

1169 Keller, G., 2003. *Guembelitria* dominated late Maastrichtian planktic foraminiferal
1170 assemblages mimic early Danian in central Egypt. Mar. Micropaleontol. 47, 71-99.
1171 https://doi.org/10.1016/S0377-8398(02)00116-0.

1172 Keller, G., Pardo, A., 2004. Disaster opportunists Guembelitrinidae: Index for environmental
1173 catastrophes. Mar. Micropaleontol. 53, 83-116.
1174 https://doi.org/10.1016/j.marmicro.2004.04.012.

1175 Keller, G., Adatte, T., Gardin, S., Bartolini, A., Bajpai, S., 2008. Main Deccan volcanism phase
1176 ends near the K-T boundary: Evidence from the Krishna-Godavari Basin, SE India. Earth
1177 Planet. Sci. Lett. 268, 293-311. https://doi.org/10.1016/j.epsl.2008.01.015.

1178 Keller, G.K., Bhowmick, P.K., Upadhyay, H., Dave, A., Reddy, A.N., Jaiprakash, B.C., Adatte,
1179 T., 2011. Deccan volcanism linked to the Cretaceous-Tertiary boundary mass extinction:
1180 New evidence from ONGC wells in the Krishna-Godavari Basin. J. Geol. Soc. India 78,
1181 399-428. https://doi.org/10.1007/s12594-011-0107-3.

1182 Keller, G., Adatte, T., Bhowmick, P.K., Upadhyay, H., Dave, A., Reddy, A.N., Jaiprakash,
1183 B.C., 2012. Nature and timing of extinctions in Cretaceous-Tertiary planktic foraminifera
1184 preserved in Deccan intertrappean sediments of the Krishna-Godavari Basin, India. Earth
1185 Planet. Sci. Lett. 341-344, 211-221. https://doi.org/10.1016/j.epsl.2012.06.021.

1186 Keller, G., Punekar, J., Mateo, P., 2016. Upheavals during the Late Maastrichtian: Volcanism,
1187 climate and faunal events preceding the end-Cretaceous mass extinction. Palaeogeogr.
1188 Palaeoclimatol. Palaeoecol. 441, 137-151. https://doi.org/10.1016/j.palaeo.2015.06.034.

1189 Keller, G., Mateo, P., Monkenbusch, J., Thibault, N., Punekar, J., Spangenberg, J.E.,
1190 Abramovich, S., Ashckenazi-Polivoda, S., Schoene, B., Eddy, M.P., Samperton, K.M.,
1191 Khadri, S.F.R., Adatte, T., 2020. Mercury linked to Deccan Traps volcanism, climate

change and the end-Cretaceous mass extinction. Glob. Planet. Change 194, 103312. https://doi.org/10.1016/j.gloplacha.2020.103312.

Kelly, D.C., Norris, R.D., Zachos, J.C., 2003. Deciphering the paleoceanographic significance of Early Oligocene *Braarudosphaera* chalks in the South Atlantic. Mar. Micropaleontol. 49, 49-63. https://doi.org/10.1016/S0377-8398(03)00027-6.

Krahl, G., Bom, M.H.H., Kochhann, K.G.D., Souza, L. V., Savian, J.F., Fauth, G., 2020. Environmental changes occurred during the early Danian at the Rio Grande Rise, South Atlantic Ocean. Glob. Planet. Change 191, 103197. https://doi.org/10.1016/j.gloplacha.2020.103197.

Kring, D.A., 2007. The Chicxulub impact event and its environmental consequences at the Cretaceous-Tertiary boundary. Palaeogeogr. Palaeoclimatol. Palaeoecol. 255, 4-21. https://doi.org/10.1016/j.palaeo.2007.02.037.

Kroon, D., Nederbragt, A.J., 1990. Ecology and paleoecology of triserial planktic foraminifera. Mar. Micropaleontol. 16, 25-38. https://doi.org/10.1016/0377-8398(90)90027-J.

Kucera, M., Malmgren, B.A., Sturesson, U., 1997. Foraminiferal dissolution at shallow depths of the Walvis Ridge and Rio Grande Rise during the latest Cretaceous: Inferences for deep-water circulation in the South Atlantic. Palaeogeogr. Palaeoclimatol. Palaeoecol. 129, 195-212. https://doi.org/10.1016/S0031-0182(96)00133-2.

Lamolda, M.A., Melinte, M.C., Kaiho, K., 2005. Nannofloral extinction and survivorship across the K/T boundary at Caravaca, southeastern Spain. Palaeogeogr. Palaeoclimatol. Palaeoecol. 224, 27-52. https://doi.org/10.1016/j.palaeo.2005.03.030.

Lamolda, M.A., Melinte-Dobrinescu, M.C., Kaiho, K., 2016. Calcareous nannoplankton assemblage changes linked to paleoenvironmental deterioration and recovery across the

Cretaceous-Paleogene boundary in the Betic Cordillera (Agost, Spain). Palaeogeogr. Palaeoclimatol. Palaeoecol. 441, 438-452. https://doi.org/10.1016/j.palaeo.2015.10.003.

Legendre, P., Gallagher, E.D., 2001. Ecologically meaningful transformations for ordination of species data. Oecologia 129, 271-280. https://doi.org/10.1007/s004420100716.

Lowery, C.M., Fraass, A.J., 2019. Morphospace expansion paces taxonomic diversification after end Cretaceous mass extinction. Nat. Ecol. Evol. 3, 900-904. https://doi.org/10.1038/s41559-019-0835-0.

Lowery, C.M., Bralower, T.J., Owens, J.D., Rodríguez-Tovar, F.J., Jones, H., Smit, J., Whalen, M.T., Claeys, P., Farley, K., Gulick, S.P.S., Morgan, J. V., Green, S., Chenot, E., Christeson, G.L., Cockell, C.S., Coolen, M.J.L., Ferrière, L., Gebhardt, C., Goto, K., Kring, D.A., Lofi, J., Ocampo-Torres, R., Perez-Cruz, L., Pickersgill, A.E., Poelchau, M.H., Rae, A.S.P., Rasmussen, C., Rebolledo-Vieyra, M., Riller, U., Sato, H., Tikoo, S.M., Tomioka, N., Urrutia-Fucugauchi, J., Vellekoop, J., Wittmann, A., Xiao, L., Yamaguchi, K.E., Zylberman, W., 2018. Rapid recovery of life at ground zero of the end-Cretaceous mass extinction. Nature 558, 288-291. https://doi.org/10.1038/s41586-018-0163-6.

Lowery, C.M., Bown, P.R., Fraass, A.J., Hull, P.M., 2020. Ecological Response of Plankton to Environmental Change: Thresholds for Extinction. Annu. Rev. Earth Planet. Sci. 48. https://doi.org/10.1146/annurev-earth-081619-052818.

Luciani, V., D'Onofrio, R., Filippi, G., Moretti, S., 2020. Which was the habitat of early Eocene planktic foraminifer *Chiloguembelina*? Stable isotope paleobiology from the Atlantic Ocean and implication for paleoceanographic reconstructions. Glob. Planet. Change 191, 103216. https://doi.org/10.1016/j.gloplacha.2020.103216.

Lyson, T.R., Miller, I.M., Bercovici, A.D., Weissenburger, K., Fuentes, A.J., Clyde, W.C., Hagadorn, J.W., Butrim, M.J., Johnson, K.R., Fleming, R.F., Barclay, R.S., Maccracken, S.A., Lloyd, B., Wilson, G.P., Krause, D.W., Chester, S.G.B., 2019. Exceptional continental record of biotic recovery after the Cretaceous−Paleogene mass extinction. Science 366, 977-983. https://doi.org/10.1126/science.aay2268.

Mateo, P., Keller, G., Adatte, T., Spangenberg, J.E., 2016. Mass wasting and hiatuses during the Cretaceous-Tertiary transition in the North Atlantic: Relationship to the Chicxulub impact? Palaeogeogr. Palaeoclimatol. Palaeoecol. 441, 96-115. https://doi.org/10.1016/j.palaeo.2015.01.019.

Metsana-Oussaid, F., Belhai, D., Arenillas, I., Arz, J.A., Gilabert, V., 2019. New sections of the Cretaceous-Paleogene transition in the southwestern Tethys (Médéa, northern Algeria): planktic foraminiferal biostratigraphy and biochronology. Arab. J. Geosci. 12. https://doi.org/10.1007/s12517-019-4402-4.

Minoletti, F., De Rafelis, M., Renard, M., Gardin, S., Young, J., 2005. Changes in the pelagic fine fraction carbonate sedimentation during the Cretaceous-Paleocene transition: Contribution of the separation technique to the study of Bidart section. Palaeogeogr. Palaeoclimatol. Palaeoecol. 216, 119-137. https://doi.org/10.1016/j.palaeo.2004.10.006.

Molina, E., Arenillas, I., Arz, J.A. 1998. Mass extinction in planktic foraminifera at the Cretaceous/Tertiary boundary in subtropical and temperate latitudes. Bull. Soc. géol. Fr. 169(3), 351-363.

Molina, E., Alegret, L., Arenillas, I., Arz, J.A., Gallala, N., Grajales-Nishimura, J.M., Murillo-Muñetón, G., Zaghbib-Turki, D., 2009. The Global Boundary Stratotype Section and Point for the base of the Danian Stage (Paleocene, Paleogene, “Tertiary”, Cenozoic): Auxiliary sections and correlation. Episodes 32, 84-95. https://doi.org/10.18814/epiiugs/2009/v32i2/002.

1263 Mukhopadhyay, S., Farley, KA., Montanari, A., 2001. A short duration of the Cretaceous-
1264 Tertiary boundary event: Evidence from extraterrestrial Helium^3. Science 291, 1952-1955.
1265 https://doi.org/10.1126/science.291.5510.1952

1266 Norris, R.D., 1996. Symbiosis as an evolutionary innovation in the radiation of Paleocene
1267 planktic foraminifera. Paleobiology 22, 461-480.
1268 https://doi.org/10.1017/S0094837300016468.

1269 Olsson, R.K., Berggren, W.A., Hemleben, C., Huber, B.T., 1999. Atlas of Paleocene Planktonic
1270 Foraminifera. Smithson. Contrib. to Paleobiol. 85, 1-252.
1271 https://doi.org/10.5479/si.00810266.85.1.

1272 Omaña, L., Alencáster, G., Hernández, J.R.T., Doncel, R.L., 2012. Morphological abnormalities
1273 and dwarfism in Maastrichtian foraminifera from the Cárdenas Formation, Valles-San
1274 Luis Potosí Platform, Mexico: Evidence of paleoenvironmental stress. Bol. Soc. Geol.
1275 Mex. 64, 305-318. https://doi.org/10.18268/BSGM2012v64n3a4.

1276 Pardo, A., Keller, G., 2008. Biotic effects of environmental catastrophes at the end of the
1277 Cretaceous and early Tertiary: *Guembelitria* and *Heterohelix* blooms. Cretac. Res. 29,
1278 1058-1073. https://doi.org/10.1016/j.cretres.2008.05.031.

1279 Pospichal, J.J., 1996. Calcareous nannoplankton mass extinction at the Cretaceous/Tertiary
1280 boundary: An update. Geol. Soc. Am. Spec. Pap. 307, 335-360. https://doi.org/10.1130/0-
1281 8137-2307-8.335.

1282 Premović, P.I., 2009. Experimental evidence for the global acidification of surface ocean at the
1283 Cretaceous-Palaeogene boundary: The biogenic calcite-poor spherule layers. Int. J.
1284 Astrobiol. 8, 193-206. https://doi.org/10.1017/S1473550409990139.

1285 Punekar, J., Mateo, P., Keller, G., 2014a. Effects of Deccan volcanism on paleoenvironment
1286 and planktic foraminifera: A global survey. Spec. Geol. Soc. Am. Spec. Pap. 505, 91-116.
1287 https://doi.org/10.1130/2014.2505(04).

1288 Punekar, J., Keller, G., Khozyem, H., Hamming, C., Adatte, T., Tantawy, A.A., Spangenberg,
1289 J.E., 2014b. Late Maastrichtian-early Danian high-stress environments and delayed
1290 recovery linked to Deccan volcanism. Cretac. Res. 49, 63-82.
1291 https://doi.org/10.1016/j.cretres.2014.01.002.

1292 Punekar, J., Keller, G., Khozyem, H.M., Adatte, T., Font, E., Spangenberg, J., 2016. A multi-
1293 proxy approach to decode the end-Cretaceous mass extinction. Palaeogeogr.
1294 Palaeoclimatol. Palaeoecol. 441, 116-136. https://doi.org/10.1016/j.palaeo.2015.08.025.

1295 Quillévéré, F., Norris, R.D., Kroon, D., Wilson, P.A., 2008. Transient ocean warming and shifts
1296 in carbon reservoirs during the early Danian. Earth Planet. Sci. Lett. 265, 600-615.
1297 https://doi.org/10.1016/j.epsl.2007.10.040.

1298 Renne, P.R., Sprain, C.J., Richards, M.A., Self, S., Vanderkluysen, L., Pande, K., 2015. State
1299 shift in Deccan volcanism at the Cretaceous-Paleogene boundary, possibly induced by
1300 impact. Science 350, 76-78. https://doi.org/10.1126/science.aac7549.

1301 Renne, P.R., Arenillas, I., Arz, J.A., Vajda, V., Gilabert, V., Bermúdez, H.D., 2018. Multi-
1302 proxy record of the Chicxulub impact at the Cretaceous- Paleogene boundary from
1303 Gorgonilla Island, Colombia. Geology 46, 547-550. https://doi.org/10.1130/G40224.1.

1304 Ricotta, C., Podani, J., 2017. On some properties of the Bray-Curtis dissimilarity and their
1305 ecological meaning. Ecol. Complex. 31, 201-205.
1306 https://doi.org/10.1016/j.ecocom.2017.07.003.

1307 Richards, M.A., Alvarez, W., Self, S., Karlstrom, L., Renne, P.R., Manga, M., Sprain, C.J.,
1308 Smit, J., Vanderkluysen, L., Gibson, S.A., 2015. Triggering of the largest Deccan

1309 eruptions by the Chicxulub impact. Bull. Geol. Soc. Am. 127, 1507-1520.
1310 https://doi.org/10.1130/B31167.1.

1311 Robinson, N., Ravizza, G., Coccioni, R., Peucker-Ehrenbrink, B., Norris, R., 2009. A high-
1312 resolution marine $^{187}Os/^{188}Os$ record for the late Maastrichtian: Distinguishing the
1313 chemical fingerprints of Deccan volcanism and the K-P impact event. Earth Planet. Sci.
1314 Lett. 281, 159-168. https://doi.org/10.1016/j.epsl.2009.02.019.

1315 Romein, A.J.T., 1977. Calcareous nannofossils from the Cretaceous/Tertiary boundary interval
1316 in the Barranco del Gredero (Caravaca, Prov. Murcia, SE Spain). Proc. K. Ned. Akad.
1317 Wet. Ser. B 80, 256-279.

1318 Schmidt, A., Skeffington, R.A., Thordarson, T., Self, S., Forster, P.M., Rap, A., Ridgwell, A.,
1319 Fowler, D., Wilson, M., Mann, G.W., Wignall, P.B., Carslaw, K.S., 2016. Selective
1320 environmental stress from sulphur emitted by continental flood basalt eruptions. Nat.
1321 Geosci. 9, 77-82. https://doi.org/10.1038/ngeo2588.

1322 Schoene, B., Samperton, K.M., Eddy, M.P., Keller, G., Adatte, T., Bowring, S.A., Khadri,
1323 S.F.R., Gertsch, B., 2015. U-Pb geochronology of the Deccan Traps and relation to the
1324 end-Cretaceous mass extinction. Science 347, 182-184.
1325 https://doi.org/10.1126/science.aaa0118.

1326 Schoene, B., Eddy, M.P., Samperton, K.M., Keller, C.B., Keller, G., Adatte, T., Khadri, S.F.R.,
1327 2019. U-Pb constraints on pulsed eruption of the Deccan Traps across the end-Cretaceous
1328 mass extinction. Science 363, 862-866. https://doi.org/10.1126/science.aau2422.

1329 Schoene, B., Eddy, M. P., Keller, C. B., and Samperton, K. M., 2021. An evaluation of Deccan
1330 Traps eruption rates using geochronologic data: Geochronology 3, 181–198.
1331 https://doi.org/10.5194/gchron-3-181-2021.

Schulte, P., Alegret, L., Arenillas, I., Arz, J.A., Barton, P.J., Bown, P.R., Bralower, T.J., Christeson, G.L., Claeys, P., Cockell, C.S., Collins, G.S., Deutsch, A., Goldin, T.J., Goto, K., Grajales-Nishimura, J.M., Grieve, R.A.F., Gulick, S.P.S., Johnson, K.R., Kiessling, W., Koeberl, C., Kring, D.A., MacLeod, K.G., Matsui, T., Melosh, J., Montanari, A., Morgan, J. V., Neal, C.R., Nichols, D.J., Norris, R.D., Pierazzo, E., Ravizza, G., Rebolledo-Vieyra, M., Reimold, W.U., Robin, E., Salge, T., Speijer, R.P., Sweet, A.R., Urrutia-Fucugauchi, J., Vajda, V., Whalen, M.T., Willumsen, P.S., 2010. The Chicxulub asteroid impact and mass extinction at the Cretaceous-Paleogene boundary. Science 327, 1214-1218. https://doi.org/10.1126/science.1177265.

Self, S., Widdowson, M., Thordarson, T., Jay, A.E., 2006. Volatile fluxes during flood basalt eruptions and potential effects on the global environment: A Deccan perspective. Earth Planet. Sci. Lett. 248, 518-532. https://doi.org/10.1016/j.epsl.2006.05.041.

Self, S., Jay, A.E., Widdowson, M., Keszthelyi, L.P., 2008. Correlation of the Deccan and Rajahmundry Trap lavas: Are these the longest and largest lava flows on Earth? J. Volcanol. Geotherm. Res. 172, 3-19. https://doi.org/10.1016/j.jvolgeores.2006.11.012.

Sepúlveda, J., Wendler, J.E., Summons, R.E., Hinrichs, K.U., 2009. Rapid resurgence of marine productivity after the Cretaceous-Paleogene mass extinction. Science 326, 129-132. https://doi.org/10.1126/science.1176233.

Sepúlveda, J., Alegret, L., Thomas, E., Haddad, E., Cao, C., Summons, R.E., 2019. Stable Isotope Constraints on Marine Productivity Across the Cretaceous-Paleogene Mass Extinction. Paleoceanogr. Paleoclimatology 34, 1195-1217. https://doi.org/10.1029/2018PA003442.

Sinnesael, M., Montanari, A., Coccioni, R., Frontalini, F., Gattacceca, J., Snoeck, C., Wegner, W., Koeberl, C., Morgan, L.E., De Winter, N.J., DePaolo, D.J., Claeys, P., 2019. Multiproxy Cretaceous-Paleogene boundary event stratigraphy: An Umbria-Marche

basinwide perspective. Geol. Soc. Am. Spec. Pap. 542, 133-158. https://doi.org/10.1130/2019.2542(07).

Smit, J., 1982. Extinction and evolution of planktonic foraminifera after a major impact at the Cretaceous/Tertiary boundary. Geol. Soc. Am. Spec. Pap. 190, 329-352. https://doi.org/10.1130/SPE190-p329.

Smit, J., 1999. The global stratigraphy of the Cretaceous-Tertiary boundary impact ejecta. Annu. Rev. Earth Planet. Sci. 27, 75-113. https://doi.org/10.1146/annurev.earth.27.1.75.

Smit, J., 2004. The section of the Barranco del Gredero (Caravaca, SE Spain): A crucial section for the Cretaceous/Tertiary boundary impact extinction hypothesis. J. Iber. Geol. 31, 179-191. https://doi.org/10.5209/JIGE.33967.

Smit, J., Hertogen, J., 1980. An extraterrestrial event at the Cretaceous-Tertiary boundary. Nature 285, 198-200. https://doi.org/10.1038/285198a0.

Smit, J., Romein, A.J.T., 1985. A sequence of events across the Cretaceous-Tertiary boundary. Earth Planet. Sci. Lett. 74, 155-170. https://doi.org/10.1016/0012-821X(85)90019-6.

Sosa-Montes de Oca, C., Rodríguez-Tovar, F.J., Martínez-Ruiz, F., 2016. Geochemical and isotopic characterization of trace fossil infillings: New insights on tracemaker activity after the K/Pg impact event. Cretac. Res. 57, 391-401. https://doi.org/10.1016/j.cretres.2015.03.003.

Sprain, C.J., Renne, P.R., Clemens, W.A., Wilson, G.P., 2018. Calibration of chron C29r: New high-precision geochronologic and paleomagnetic constraints from the Hell Creek region, Montana. Bull. Geol. Soc. Am. 130, 1615-1644. https://doi.org/10.1130/B31890.1.

1378 Sprain, C.J., Renne, P.R., Vanderkluysen, L., Pande, K., Self, S., Mittal, T., 2019. The eruptive
1379 tempo of Deccan volcanism in relation to the Cretaceous-Paleogene boundary. Science.
1380 363, 866-870. https://doi.org/10.1126/science.aav1446.

1381 Stax, R., Stein, R., 1993. Long-term changes in the accumulation of organic carbon in Neogene
1382 sediments, Ontong Java Plateau. Proc., Sci. results, ODP, Leg 130, Ontong Java Plateau
1383 130, 573-584. https://doi.org/10.2973/odp.proc.sr.130.039.1993.

1384 Steinthorsdottir, M., Vajda, V., Pole, M., 2016. Global trends of pCO_2 across the Cretaceous-
1385 Paleogene boundary supported by the first Southern Hemisphere stomatal proxy-based
1386 pCO_2 reconstruction. Palaeogeogr. Palaeoclimatol. Palaeoecol. 464, 143-152.
1387 https://doi.org/10.1016/j.palaeo.2016.04.033.

1388 Thibault, N., Gardin, S., 2010. The calcareous nannofossil response to the end-Cretaceous warm
1389 event in the Tropical Pacific. Palaeogeogr. Palaeoclimatol. Palaeoecol. 291, 239-252.
1390 https://doi.org/10.1016/j.palaeo.2010.02.036.

1391 Thibault, N., Galbrun, B., Gardin, S., Minoletti, F., Le Callonnec, L., 2016. The end-Cretaceous
1392 in the southwestern Tethys (Elles, Tunisia): orbital calibration of paleoenvironmental
1393 events before the mass extinction. Int. J. Earth Sci. 105, 771-795.
1394 https://doi.org/10.1007/s00531-015-1192-0.

1395 Thibault, N., Minoletti, F., Gardin, S., 2018. Offsets in the early Danian recovery phase in
1396 carbon isotopes: Evidence from the biometrics and phylogeny of the *Cruciplacolithus*
1397 lineage. Rev. Micropaleontol. 61, 207-221. https://doi.org/10.1016/j.revmic.2018.09.002.

1398 Tobin, T.S., Bitz, C.M., Archer, D., 2017. Modeling climatic effects of carbon dioxide
1399 emissions from Deccan Traps volcanic eruptions around the Cretaceous-Paleogene
1400 boundary. Palaeogeogr. Palaeoclimatol. Palaeoecol. 478, 139-148.
1401 https://doi.org/10.1016/j.palaeo.2016.05.028.

1402 Vandamme, D., Courtillot, V., Besse, J., Montigny, R., 1991. Paleomagnetism and age
1403 determinations of the Deccan traps (India): results of a Nagpur–Bombay traverse and
1404 review of earlier work. Rev. Geophys. Space Phys. 29, 159–190.

1405 Vellekoop, J., Sluijs, A., Smit, J., Schouten, S., Weijers, J.W.H., Sinninghe Damsté, J.S.,
1406 Brinkhuis, H., 2014. Rapid short-term cooling following the Chicxulub impact at the
1407 Cretaceous-Paleogene boundary. Proc. Natl. Acad. Sci. USA 111, 7537-7541.
1408 https://doi.org/10.1073/pnas.1319253111.

1409 Vellekoop, J., Esmeray-Senlet, S., Miller, K.G., Browning, J. V, Sluijs, A., van de
1410 Schootbrugge, B., Sinninghe Damsté, J.S., Brinkhuis, H., 2016. Evidence for Cretaceous-
1411 Paleogene boundary bolide "impact winter" conditions from New Jersey, USA. Geology
1412 44. https://doi.org/10.1130/G37961.1.

1413 Vellekoop, J., Woelders, L., van Helmond, N.A.G.M., Galeotti, S., Smit, J., Slomp, C.P.,
1414 Brinkhuis, H., Claeys, P., Speijer, R.P., 2018. Shelf hypoxia in response to global warming
1415 after the Cretaceous-Paleogene boundary impact. Geology 46, 683-686.
1416 https://doi.org/10.1130/G45000.1.

1417 Wade, B.S., Pearson, P.N., Berggren, W.A., Pälike, H., 2011. Review and revision of Cenozoic
1418 tropical planktonic foraminiferal biostratigraphy and calibration to the geomagnetic
1419 polarity and astronomical time scale. Earth-Science Rev. 104, 111-142.
1420 https://doi.org/10.1016/j.earscirev.2010.09.003.